SBN Oscillation Sensitivity Calculations (2019z)

Authors

Institutes

Abstract

Keywords:

Contents

Preprint submitted to Journal Name *September 27, 2022*

1. Introduction

2. Oscillation Analysis Paradigm

3. Monte Carlo Event Simulation

3.1. ν_μ Production

The samples used in the ν_μ event selection (see section 4.1) are 1 million BNB MC events produced in each detector. The beam is in the default configuration – including all muon and intrinsic electron neutrinos and including pileup. Each neutrino interaction also has 1000 "universes" of each systematic parameter (as documented below) calculated.

TODO: Document specific versions and configurations

3.2. ν_e Production

TODO: Add The Appendix TODO: Make Beam 1/r sqrd figure TODO: figure labels

3.2.1. Producing the Modern Sample

The SBN Programme expects to take 6.6e20 protons on target (POT) of data for the near and far detector and 13.2 POT for MicroBooNE. This corresponds approximately 7 million ν_μ events and 500 k intrinsic ν_e events in the SBND detector. For the ν_e analysis the oscillated ν_e signal is $\mathcal{O}(100)$ events in the SBND Detector for the global best fit parameters for the 3+1 sterile model, $\sin^2(\theta_{\mu e}) = 0.003$ and $\Delta m^2_{41} = 1.2\ eV^2$. The charge current intrinsic ν_e make up $\sim$0.5% of the beam with $\sim$300 K events in the SBND detector. Resonant neutral current ν_μ with a final state neutral pion events which are one of the main backgrounds in the analysis account for $\sim$12% of the ν_μ events. In order to minimise statistical fluctuations and still be within the computational means of the experiment 1 million BNB-like events were created using the event generator GENIE in the LArSoft framework. The BNB-like neutrino events generated using GENIE have the exact beam composition of the BNB. Note that the simulation also includes meson exchange current (MEC) interactions which correspond to neutrino interactions with a pair of hadrons.

A dedicated intrinsic ν_e sample of 1 million events was also produced. This was necessary as only $\sim$0.5% ($\sim$50 K) of the BNB-like sample corresponds to the charge current intrinsic ν_e. This is $\sim$10% of the intrinsic events over the 3 year run. A further 1 million BNB-like events were generated with their flavour swapped to mimic the oscillation signal. A oscillation weight is then applied within the fitting frameworks, see section **??**. For the global best fit of 3+1 sterile hypothesis of $\sin^2(\theta_{\mu e}) = 0.003$ and $\Delta m^2 = 1.2\ eV^2$ the oscillation probability at the SBND detector at approximately the peak BNB energy (110 m Baseline at 1 GeV) is $\sim$4e-4. The oscillation probability is given as weight to the event and therefore the sample has a weight corresponding to $\mathcal{O}(100)$ events. The samples were produced in all 3 detectors corresponding to a total of 9 million events.

The events also underwent event re-weighting. Re-weighting involves throwing physical quantities within the uncertainty of the quantity randomly from an assumed Gaussian or uniform distribution. The events are then regenerated with the physical parameters corresponding to the new values of the physical quantities. The throwing is done several times to provide several possible universes. Each universe is then provided with a probability from the GENIE re-weighting framework. The uncertainty on the physical parameter is then carried through to the sensitivity analysis by the generated Universes models. Tables 5.2 & 5.1 show the systematic errors on the physical quantities that were considered in the event re-weighting. CAN SOMEONE WITH MORE KNOWLEDGE ADD OR CORRECT THIS PLEASE.

The simulation generates events through a flux window of 10 m X 10m, 10 m upstream of the front face of the detector, which ensures the the majority of the events occur within the detector or nearby. A further 100 K BNB-like events were generated with a larger flux window of 80 m x 80 m, at the face of the detector, to incorporate more interactions that occur outside of the detector. Events where particles from these external interactions propagate into the detector are known as dirt events and when a high energy photon propagates into the detector and pair produces the event can mimic a charge current interaction where 0 track-like (muon, proton, charged kaon, charged pion) final state particles are emitted from the vertex.

The events are overlaid with cosmic events generated by Corsika. A Cosmic event can mimic the charge current event if a high energy cosmic photon interacts within the detector. During the 3 year run time of the experiment it expected that 211 seconds of beam spill data. 100 K of cosmic overlaid, dirt events correspond to ~ 0.04 % of the events in the three year run. The spill time from the BNB beam is 1200 ns therefore 0.12 of in-time cosmics were generated in the sample. The selection analysis in section 4.2 assumes that if the cosmic event occurred out of the beam spill window the cosmic is tagged 100% of the time by either the Photon Detection System (PDS) or the Cosmic Ray Tagging system (CRT). Therefore to improve the statistics of the comic events all events in the drift window (3 ms for SBND) were considered. A scale factor of the beam spill time divided by drift window was then applied to the cosmic events. This increased the sample to $\sim$300 s of data. As the statistics are low for this sample future evaluations of the sensitivity must ensure more events are simulated to improve the statistics of the analysis.

The events described here are then defined as the ”modern” sample. The next section will describe how the ”modern” sample is altered to produce the ”proposal” sample.

3.2.2. Producing the Proposal Samples

To produce a proposal era sample the modern sample is taken and individual weights are applied to the events. Firstly SBND has moved since the proposal era from 100 m to 110 m. To account for this a weight of 1.21 is applied to all SBND events in the modern sample to correct for the change in the flux due to the position. This assumes the beam is uniformly emitted in as a cone. Figure **??** depicts the movement of the detector and the corresponding effect on the flux.

A weight is also applied to the event depending on its nuisance interaction mode as a function of the neutrino energy. The weight is applied to account for changes in the physic model from GENIE version v2_8 to v2_12. There are several changes to the model which are documented in the GENIE version release notes. There have been small tweaks in the resonant models in version v2_12 and minor bug fixes in coherent pion model in version v2_8_2. In v2_10 there was a re-tune of the parameters for producing the DIS cross section spline. The GENIE release notes do not give further information on the physical changes that are resultant from the these updates. Additional changes in other contexts can be found in the release notes. Changes in the Flux during this era were not considered in the analysis. *Zarko mentions changes to the Kaon flux of a few % in previous talks. I don't know if this is accounted for in the flux files used.*

200 K BNB-like events were generated using v2_8 and v2_12. The difference between the samples was calculated for the nuisance interaction modes. For the ν_e selection the nuisance modes that are important when considering the signal are charge current events where the electron candidate is visible. Quasi-elastic charge current events with 0 final state charge pions (CC0π), Figure 1, are the most common events corresponding to approximately 62% (with MEC events removed) of the charge current events. There is a 6.3% decrease in the total event rate of CC0π events from the BNB from the modern era (v2_12) to the proposal era (v2_8) and as can be seen in Figure 1 this loss is relatively constant as function of the neutrino Energy.

Resonant interaction where a charge pion is created, Figures 2(a), 2(b) and **??** correspond to 28.9% of the events and there is 10.0% decrease in events in the proposal era compared to the modern era samples. Contributions from other charge current interaction modes can be found in Appendix **??** table **??**. One the main backgrounds for a ν_e selection is a misidentified photon shower arising from a final state neutral pion decay in a neutral current interaction. Figures 3(a) to 3(d) correspond Neutral current interaction modes which can produce a neutral pion in the final state. There is a global loss of 7.7% from the modern sample to the proposal sample for neutral current resonant events, with a final state neutral pion, Figures 3(a) and 3(b). There is also a global 2.5% increase in DIS interactions, Figure 3(c) as well as 11.3% increase in Coherent Scattering Interactions, Figure 3(d). Differences in the GENIE versions are considered for interactions with $\nu_m u$ particles. However the weights shown are applied to both $\nu_m u$ and ν_e interactions. Additional studies should be made account for difference in ν_e interactions.

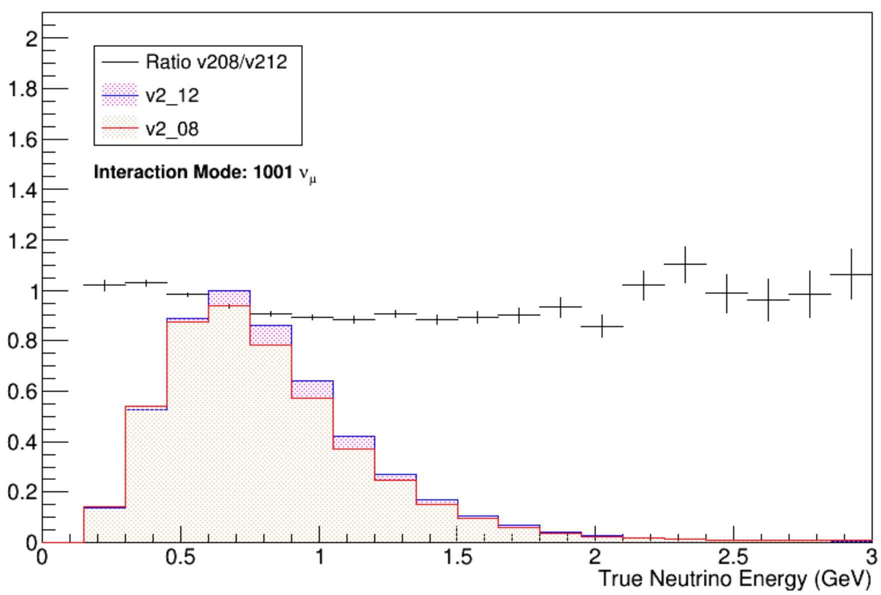

Figure 1: The interaction rates of CC0Pi events in GENIE v2_8 and v2_12. The errors on the plot are statistical

Additional studies were made to identify changes in the rate and energy of final state particles. Hadronic final state particles are used to identify the neutrino vertex and identifying the vertex correctly is useful for removing the neutral current background. Neutral current events with a photon propagating from the vertex can be misidentified as a charge current electron neutrino event when the photon shower is misidentified as the lepton shower. However,

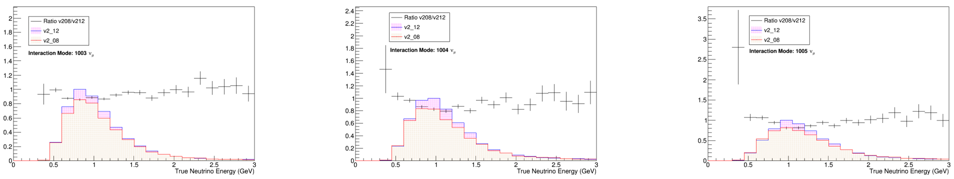

Figure 2: Figures showing the differences in rates of Charge Current Resonant Interaction types from GENIE version v2_12 and v2_8.1 a) Charge Current Resonant interaction on a proton producing a final state positively charge pion. b) Charge Current Resonant interaction on a proton producing a final state neutral pion. c) Charge Current Resonant interaction on a neutron producing a final state positively charge pion.

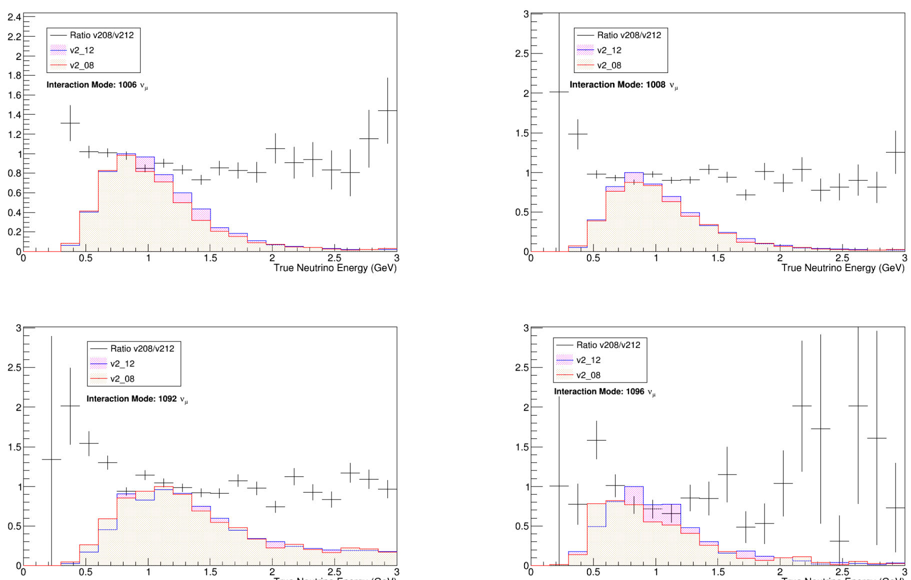

Figure 3: Figures showing the differences in rates of Neutral current interactions between GENIE versions v2_12 and v2_8. Note that a neutral pion is not always created in DIS and Coherent scattering events. a) Charge Current Resonant interaction on a proton producing a final state positively charge pion. b) Neutral Current Resonant interaction on a proton producing a final state neutral pion. c) Neutral Current Deep Inelastic Scattering Events. d) Neutral Current Coherent Scattering events

photons can travel several centimeters in liquid argon without interacting or decaying and as the photons do not ionise the liquid argon there can be a physical gap, known as the conversion distance, between the neutrino vertex and the shower vertex. This is not the case for the electron shower and hence the events can be removed if the conversion gap is visible.

Figures 4(a) and 4(b) show the ratio between the total final state hadronic energy at the vertex of the different GENIE versions after corrections are applied to account for the difference in interaction rates described above. The interaction rate corrections are applied for all other final state particle properties described below. Figure 4(a) corresponds to the neutral current resonant events where the neutrino interacts with a proton and a final state neutral pion is produced which is given an interaction number of 1006. Figure 4(b) corresponds events which underwent a neutral current DIS interactions which is given the interaction number 1092.

The ratio of the hadronic energy at the vertex is approximately consistent between the two versions. Other interaction modes are considered in Appendix **??** along with a breakdown of the difference between proton energy and multiplicity and pion energy and multiplicity. This is done for all interaction modes.

The difference between the conversion distance can be seen in Figures 5(a) and 5(b) (interaction types 1006 and 1092) where it is shown that the different GENIE versions are approximately consistent. Investigations were also made into the changes in the neutral pion energy, Figure 6(a) for interaction type 1006 and Figure 6(b) for interaction type 1092, where the two versions were shown to be consistent. In addition, changes in the distribution of the energy of the neutral decay photons was considered.

Figures 7(a) and 8(a) for interaction type 1006 and Figure 7(b) and 8(b) for interaction type 1092, show the changes in the primary photon energy and the secondary photon energy respectively. The primary and secondary photons are the photons with the highest and second highest energy coming from the vertex respectively. Changes in the primary photon energy are important when considering changes in the background event spectra. Primary photons are misidentified as electron lepton showers in the analysis and so contribute to the total neutrino energy. Changes in secondary shower energies are also important for the proposal selection as it can impact the effectiveness of the cut on events where more than one shower above 100 MeV exists in the event.

The figures indicate the GENIE versions are consistent over the majority

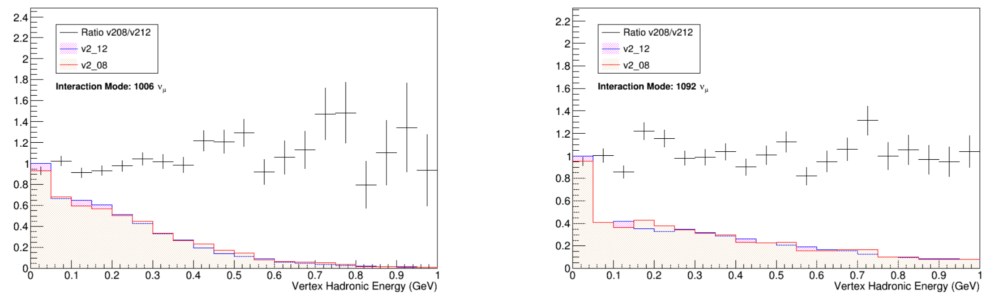

Figure 4: Figures showing the differences in the hadronic energy of neutral current interactions between GENIE versions v2_12 and v2_8. Errors are statistical Poissonain errors a) Charge Current Resonant interaction on a proton producing a final state positively charge pion. b) Neutral Current DIS Interactions.

of the distributions. Other interaction modes are considered in appendix **??**. As the properties of the final state particles are roughly consistent between the GENIE versions, no additional weights were applied. A more in depth analysis with dedicated productions of rare modes should be considered to verify these findings.

MEC events were not generated at the time the SBN proposal was produced. Therefore all MEC events were removed from the samples during the selection to produce the 'proposal era' samples. As the addition of the MEC events increases the overall cross-section of the neutrino interactions, no re-scaling of the interactions rates needs to be considered. THIS SEEM UNUSUAL TO ME CAN A EXPERT PLEASE CHECK THIS STATEMENT.

4. Event Selections and Assumed Performance

4.1. Selection of Muon-Neutrino Charged-Current Events

The ν_μ "event selection" documented here is an attempt at replicating the analysis in the SBN proposal: a truth-based study with some simulated reconstruction effects. The analysis includes such effects as neutrino energy reconstruction smearing/bias and reconstruction efficiency of signal events. In does not incorporate important effects such as the impact of cosmic muons as a background in the analysis. Differences in MC generation between the SBN proposal era and now (such as differing Genie version and a different flux simulation and detector size for SBND) cause discrepancies in the updated analysis that are partially accounted for by simple scaling of certain

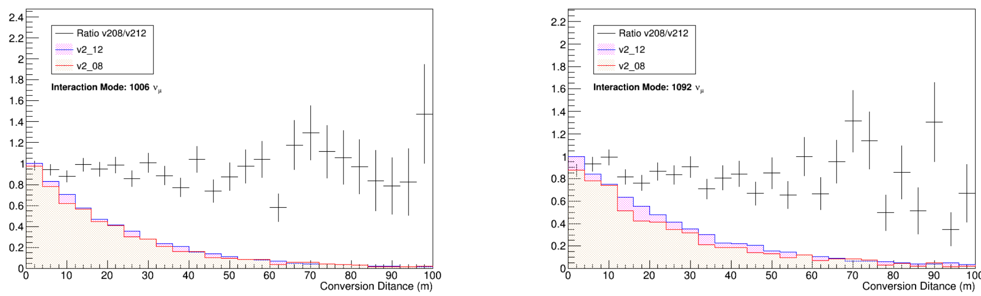

Figure 5: Figures showing the differences in the conversion distance of the most energetic photon arising from vertex interaction of neutral current interactions between GENIE versions v2_12 and v2_8. Errors are statistical Poissonain errors a) Charge Current Resonant interaction on a proton producing a final state positively charge pion. b) Neutral Current DIS Interactions.

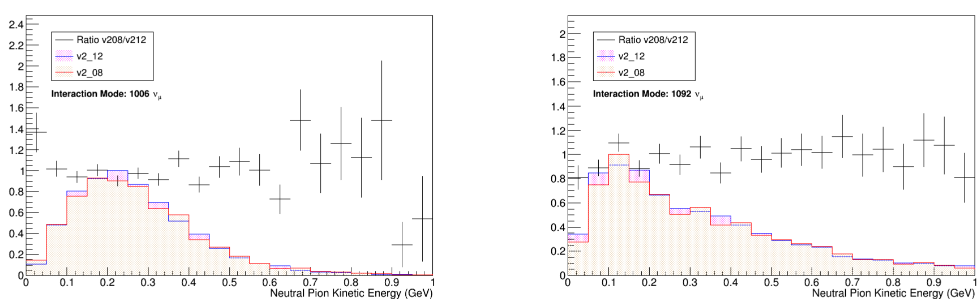

Figure 6: Figures showing the differences in the energy of a final state neutral pion in neutral current interactions between GENIE versions v2_12 and v2_8. Errors are statistical Poissonain errors a) Charge Current Resonant interaction on a proton producing a final state positively charge pion. b) Neutral Current DIS Interactions.

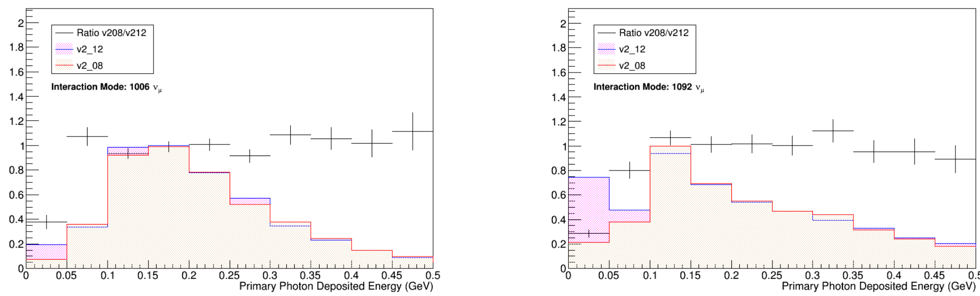

Figure 7: Figures showing the differences in the energy most energetic photon arising from the vertex in neutral current interactions between GENIE versions v2_12 and v2_8. Errors are statistical Poissonain errors a) Charge Current Resonant interaction on a proton producing a final state positively charge pion. b) Neutral Current DIS Interactions.

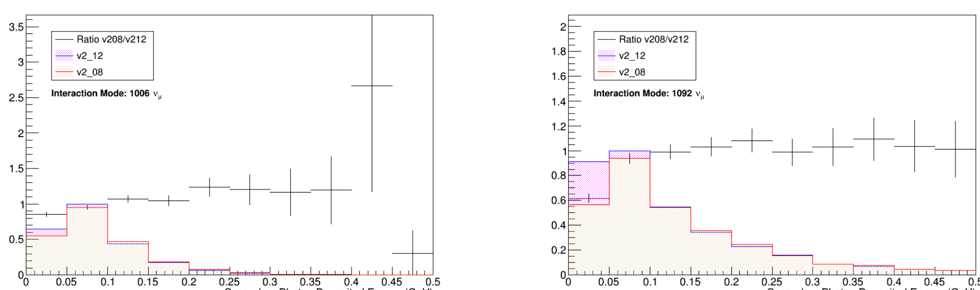

Figure 8: Figures showing the differences in the energy of the second most energetic photon arising from the vertex of a neutral current interactions between GENIE versions v2_12 and v2_8. Errors are statistical Poissonain errors a) Charge Current Resonant interaction on a proton producing a final state positively charge pion. b) Neutral Current DIS Interactions.

classes of events (as will be detailed below). There are thus two versions of the event selection: a "Proposal" version (which includes these scalings) and a "Modern" version (which does not). The "Proposal" selection represents a best attempt at completely reproducing the SBN proposal analysis. The "Modern" selection represents the expectation of a truth-based study using a more updated expectation of the neutrino flux/interaction modeling in SBN. The "Proposal" configuration spectra are shown in figure 9 (with a comparison to the SBN proposal spectra). The "Modern" configuration spectra are shown in figure 11 (with a comparison to the "Proposal" configuration spectra).

The main differences between the Modern and Proposal selections are:

1. Modern samples include Meson-Exchance Current (MEC) events ($\sim +25\%$ in all detectors)
2. Modern samples put SBND at the 110m baseline instead of 100m (-21% in SBND)
3. Modern samples have SBND with a beam-dimension length of 5m (3.65m for the Proposal sample) ($\sim +50\%$ in SBND)
4. Modern samples do not include the 1.031x upward energy scale shift. This does not change the overall normalization but does mean the energy scale of the spectra is lower compared to the Proposal sample.

The major performance assumptions of the analysis are:

1. 80% signal selection efficiency
2. No background contamination from cosmic muons
3. 2% energy reconstruction resolution for contained muon tracks
4. About 20% energy reconstruction resolution for exiting muon tracks (the exact amount is a function of the contained particle length specified below) as taken from a study in ICARUS
5. 5% energy reconstruction resolution for all hadronic tracks
6. Identification of hadronic particle tracks exactly above a deposted energy of 21MeV
7. Perfect particle ID separation between protons/muons/kaons

4.1.1. Proposal Event Selection Recipe

Cuts in the analysis:

1. Start with the samples as specified in section 3.

2. Remove all interactions with a true vertex position outside the fiducial volume definition (table 3)
3. Remove all interactions that do not produce a muon or pion particle (using the true particle ID). For interactions with such a particle, define the "primary track" as the longest such muon or pion particle emanating from the interaction vertex. Note that this definition allows for background NC events that produce a pion to enter the selection.
4. Remove all interactions with an exiting (contained) primary track with a length less than 100cm (50cm). An exiting track is one that leaves the detector active volume (table 1).
    (a) The length of this track is the distance from the start to the end point of the track inside a volume with a 5cm inset from the border of the active volume definition (table 1).
5. Remove all interactions that were produced through the MEC (Meson exchange current) process (e.g. the simb::kMEC enum value)

The single reconstructed kinematic variable in the selection is a simulated-reconstruction neutrino energy. This energy is the sum of all charged hadronic track-like particles (protons, pions, and kaons) with a kinetic energy of at least 21MeV smeared (individually) by 5%, plus the energy of any exiting (contained) muon meared by $-0.102 \cdot \log(\text{length[cm]} \cdot 0.000612)\%$ (2%). The contained smearing is to emulate a range or calorimetric based energy reconstruction, while the exiting resolution is to emulate a MCS based energy reconstruction. The particle length is defined as in the above list.

This final energy value is scaled up by 1.031 to account for an apparent energy scale shift between the SBN proposal and the reproduced spectra (see figure 10.

The output events from the selection must also be scaled by the following values:

1. All CC events by 0.8 (to emulate an 80% selection efficiency)
2. Apply the bnbcorrection weight to the ICARUS and μBooNE samples to account for a bug in their flux files.
3. Scale all CC events by 0.981 and all NC events by 1.043 (to account for changes in Genie cross section values since the proposal)
4. Scale all events in SBND by 1.21. (This partially accounts for moving the SBND baseline from 100m (proposal era flux) to 110m (reproduction flux). The reproduction is partial because the beam is a line source

and parallax effects change the event rate scaling from being a simple $1/r^2$ effect.

The output spectra from this procedure are shown in figure 9, with a comparison to the actual SBN proposal spectra.

4.1.2. Modern Event Selection Recipe

Cuts in the analysis:

1. Start with the samples as specified in section 3.
2. Remove all interactions with a true vertex position outside the fiducial volume definition (table 4)
3. Remove all interactions that do not produce a muon or pion particle (using the true particle ID). For interactions with such a particle, define the "primary track" as the longest such muon or pion particle emenating from the interaction vertex. Note that this definition allows for background NC events that produce a pion to enter the selection.
4. Remove all interactions with an exiting (contained) primary track with a length less than 100cm (50cm). An exiting track is one that leaves the detector active volume (table 2).
   (a) The length of this track is the sum of the length of each line segment connecting successive particle trajectory points as reported by G4.

The single reconstructed kinematic variable in the selection is a simulated-reconstruction neutrino energy. This energy is the sum of all charged hadronic track-like particles (protons, pions, and kaons) with a kinetic energy of at least 21MeV smeared (individually) by 5%, plus the energy of any exiting (contained) muon meared by $-0.102 \cdot \log\left(\text{length[cm]} \cdot 0.000612\right)\%$ (2%). The contained smearing is to emulate a range or calorimetric based energy reconstruction, while the exiting resolution is to emulate a MCS based energy reconstruction. The particle length is defined as in the above list.

The output events from the selection must also be scaled by the following values:

1. All CC events by 0.8 (to emulate an 80% selection efficiency)
2. Apply the bnbcorrection weight to the ICARUS and μBooNE samples to account for a bug in their flux files.

The output spectra from this procedure are shown in figure 11, with a comparison to the "Proposal" configuration spectra.

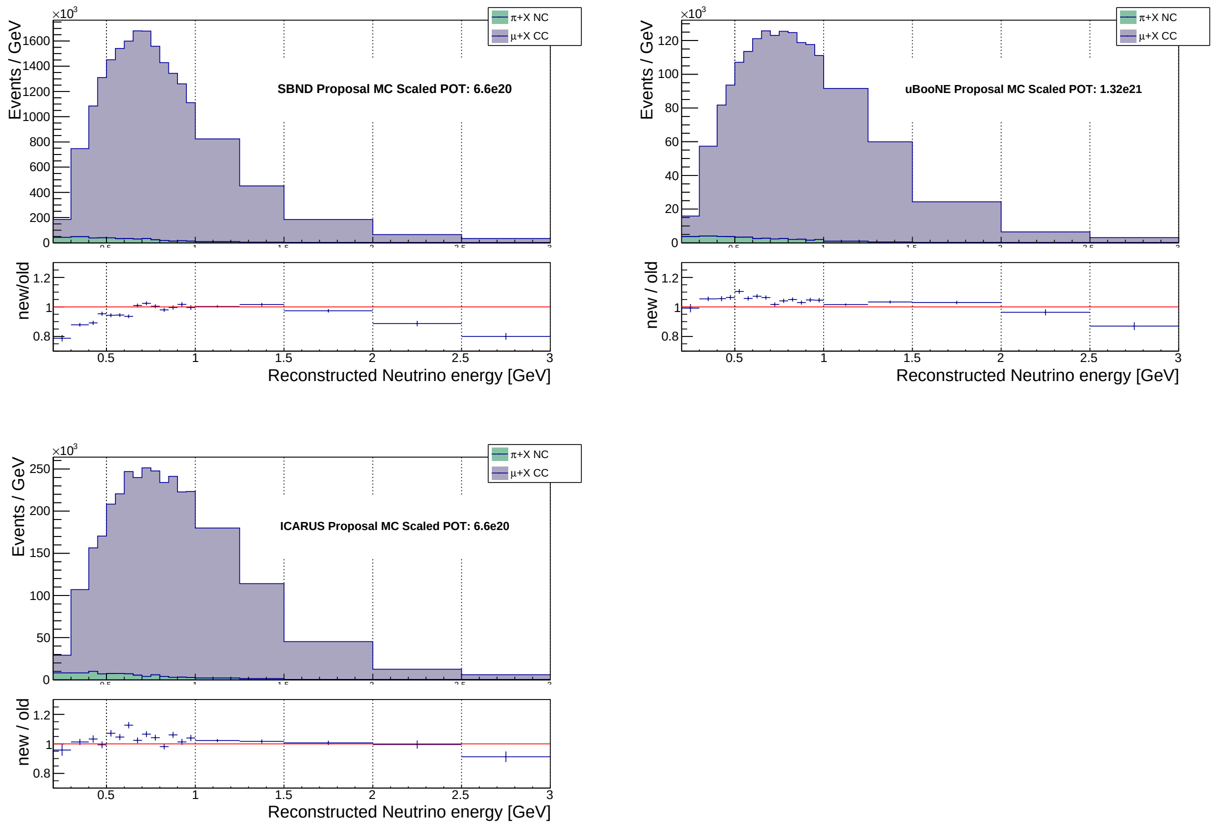

Figure 9: Event Spectra in the "Proposal" configuration in each detector (top) with a ratio to the equivalent spectra in the actual SBN proposal paper (bottom).

4.1.3. Implementation

TODO

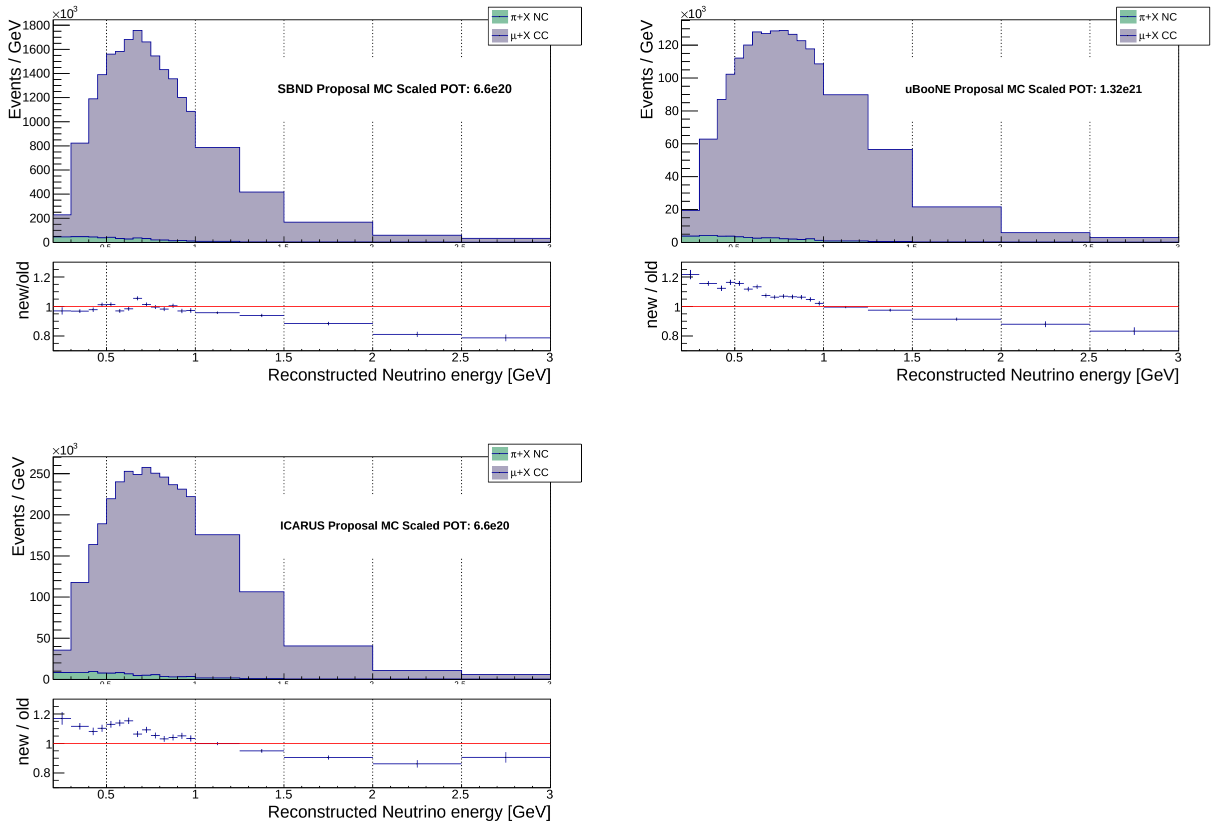

Figure 10: Event Spectra in the "Proposal" configuration in each detector (without the energy-scale shift applied) (top) with a ratio to the equivalent spectra in the actual SBN proposal paper (bottom).

Table 1: Proposal Sample Active Volumes in local detector coordinates [cm].

Detector	x_{min}	x_{max}	y_{min}	y_{max}	z_{min}	z_{max}
SBND	-199.15	199.15	-200	200	0	365
μBooNE	-1.55	254.8	-115.53	117.47	0.1	1036.9
ICARUS A	-364.49	-67.94	-173.41	143.41	-909.951	879.951
ICARUS B	67.94	364.49	-173.41	143.41	-909.951	879.951

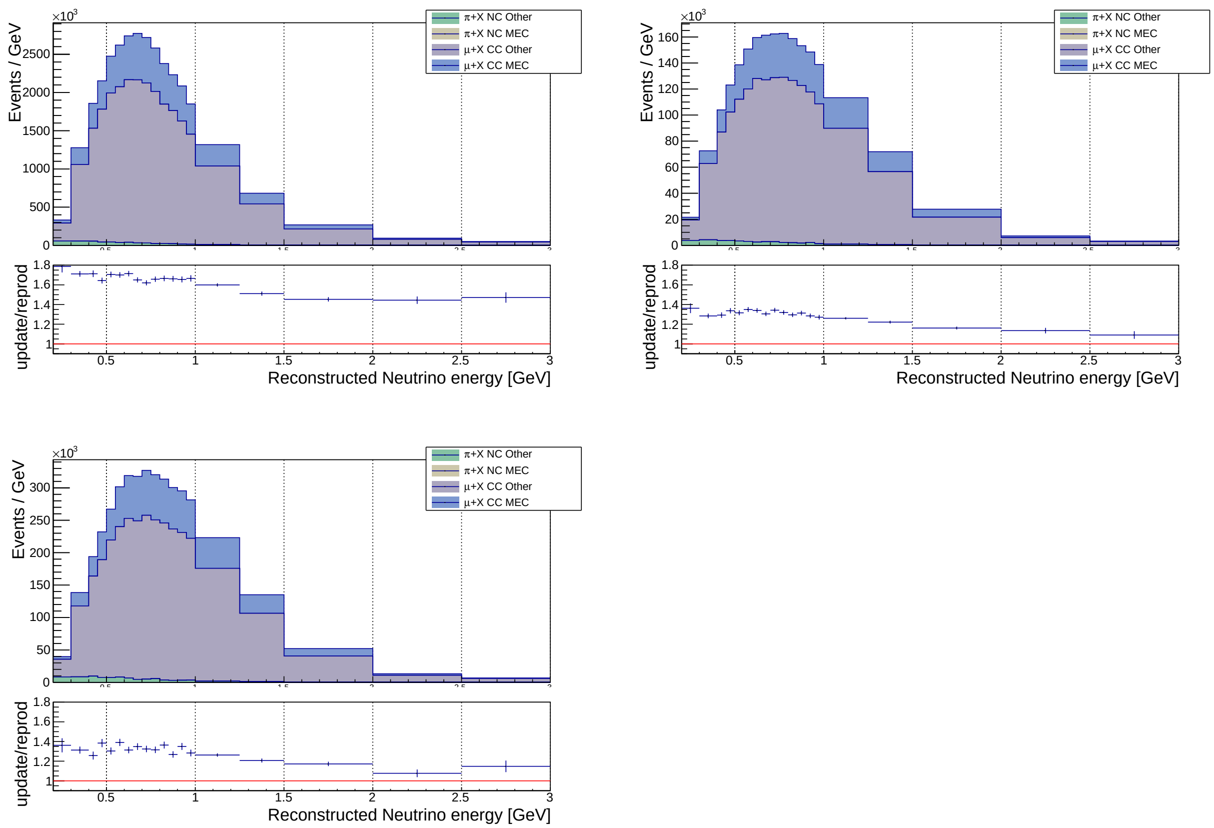

Figure 11: Event Spectra in the "Modern" configuration in each detector (top) with a ratio to the equivalent spectra in the "Proposal" configuration (bottom).

Table 2: Modern Sample Active Volumes in local detector coordinates [cm].

Detector	x_{min}	x_{max}	y_{min}	y_{max}	z_{min}	z_{max}
SBND	-199.15	199.15	-200	200	0	500
μBooNE	-1.55	254.8	-115.53	117.47	0.1	1036.9
ICARUS A	-364.49	-67.94	-173.41	143.41	-909.951	879.951
ICARUS B	67.94	364.49	-173.41	143.41	-909.951	879.951

Table 3: Proposal Sample Fiducial Volumes in local detector coordinates [cm].

Detector	x_{min}	x_{max}	y_{min}	y_{max}	z_{min}	z_{max}
SBND	-184.15	184.15	-185	185	15	285
μBooNE	13.45	239.8	-100.53	102.47	15.1	956.9
ICARUS A	-349.49	-82.94	-158.41	128.41	-894.951	799.951
ICARUS B	82.94	349.49	-158.41	128.41	-894.951	799.951

Table 4: Modern Sample Fiducial Volumes in local detector coordinates [cm].

Detector	x_{min}	x_{max}	y_{min}	y_{max}	z_{min}	z_{max}
SBND	-184.15	184.15	-185	185	15	420
μBooNE	13.45	239.8	-100.53	102.47	15.1	956.9
ICARUS A	-349.49	-82.94	-158.41	128.41	-894.951	799.951
ICARUS B	82.94	349.49	-158.41	128.41	-894.951	799.951

4.2. Selection of Electron-Neutrino Charged-Current Events

TODO WARNING DOM HAS NOT READ THROUGH THIS YET AND YOU WILL NOT BE SURPRISED HIS ENGLISH IS WOEFUL. READ AT YOUR OWN RISK .FIGURES NEED ADDING, REFERENCE NEED DOING...

The truth based selection uses the simulation to produce pseudo-reconstruction parameters in order to the perform the analysis. The signal and background are treated separately in the analysis as it was done for the proposal. The following sections will discuss the beam related signal and backgrounds together followed by Dirt-Events are treated and finally the cosmic background.

4.3. Beam Induced Signal and Background Events

Firstly the non-Dirt based samples an active volume cut is applied to the vertex to remove all events which do not interact in the liquid argon. After the the vertex has been identified in the active volume any photons originating from the vertex are found. This is done by considering all photons in the event and identifying the particle that was source particle tree. In most cases this is a final state particle from the neutrino interaction such as neutral pion. If the source particle is within 5 cm of the vertex the photon is identified as originating from the neutrino. Electrons are also identified as lepton candidates by considering electrons which originated within 5 cm of the vertex. The energy of the electron and photons is found by smearing the summation of the ionisation depositions within the simulation. The shower energy is smeared by taking a random value from a Gaussian with a mean of the energy deposited and a standard deviation of $0.15sqrt(E)$. This is in order to mimic the reconstruction affects on the energy and allows for a resolution on the shower energy of $15\%/sqrt(E)$. If a more than one photon with a smeared energy above 100 MeV exists the event is removed. This cut exists to remove neutral pion events where the pion decays into two photons showers. If one of the showers is missed by the reconstruction the remaining photon can mimic and charge current nu_e event. This cut also removes events where there is a photon with a smeared energy above 100 MeV and electron lepton candidate with a smeared energy above 100 MeV. The effectiveness of this cut at removing background can be seen in efficiency curve in Figure BLAR. Figure BLAR replicates this cut in reconstruction and compares simulated oscillated signal events and nu_μ bnb-like events with a neutral pion background in the SBND detector. Both sample have no cosmic overlay so the reconstruction is not affected by the presense of cosmics. Due to segmentation of showers one true shower can be mistaken for several showers. The Figure indicates the best place to place a cut on the shower energy to consider it an actual shower. Events are remove when more than one shower has an energy greater than cut off. The best cut off was found to be at 210 MeV giving an efficiency of BLAR and background rejection of the BLAR. This also removes events where there is no showers above the cut off. This therefore acts as an energy cut of as well and as can be seen in Figure BLAR the signal efficiency loss in the cut is predominately down to cut on the energy of the shower as X% amount of the signal is removed when events are removed that are below 210 MeV. A further 10% of the signal is lost as there is no shower the event as can be seen in Figure BLAR.

If there is only one photon candidate in the event a conversion gap cut is applied. As described above photons can travel several centimeters from the vertex before they interact or decay, see Figure BLAR. The gap between the vertex and the start position of the photon shower is the conversion gap and does not exist for electron showers. If vertex is deemed visible and the photon starts to shower further than 3 cm from the vertex the event is removed. A vertex is deemed visible if has 50 MeV of hadronic energy. Particles contribute to the visible hadronic energy if they charged either proton, pion or kaon, not a nuclear fragments, deposit for then 8.3 KeV of energy in the detector and originate from the vertex. All particles which are not leptons or photons are considered in the total vertex energy when calculating the neutrino energy. To identify if they originate from the vertex a similar method is applied to that of the photons above. The origin particle is identified by consider the particle tree. If the origin particle was created within 5 cm of the vertex the particle is identified with the vertex. The energy of each particle is then calculated by smearing the energy deposited by the particle by 5%. The efficiency of cut conversion gap cut of removing background can be seen in Figure BLAR and produced a global background rejection of BLAR. This cut does not take place on the electron candidate providing a 100% signal efficiency. Figure BLAR shows the effective the cut in actual reconstruction in SBND for a signal of oscillated ν_e and and ν_μ events with a pizero present with the best cut at BLAR corresponding to an efficiency of BLAR and background rejection of BLAR.

The remaining photon background undergoes then a dE/dx cut. When a photon interacts it usually undergoes pair production where a e^+e^- pair are produced. These are usually relativistic and forward going so they produce a single track in the liquid argon, as identified in Figure BLAR. Both particle deposit energy that is representative of the landau distribution that peaks at $sim1.9$ MeV/cm. The contribution produces a peak around $\sim$3.8 MeV/cm. This is different two that of a single electron shower which produces the the peak at around $sim1.9$ MeV/cm. Therefore placing a cut on the dE/dx, for example Figure BLAR, can remove the majority of photons showers. Some photons however undergo Compton scattering where one electron is produced. Events such as these are indistinguishable from the charge current signal. Figure BLAR in section BLAR shows and example of the separation of the median dE/dx over 3 cm using the TRACS software. A weight of 0.06 is applied to the neutral current background to account for the dEdx cut. The weight arises from studies performed in ArgonNEUT CHECK FORM where a $e\gamma$ separation was performed on selected events resulting in a background rejection of 94% and Signal Efficiency of 80%. A weight of 0.8 is not applied to the signal giving a signal efficiency of 100%. Furthermore it should be noted that the analysis was performed in the NuMi beam which has a higher energy than the BNB. Combining with the selection performed before the separation will result in higher energy photons than that of this analysis. Pair production dominates more as the energy of the photon increases and therefore more photons undergoing Compton interaction should be expected in the analysis, reducing the background rejection.

If a misidentified photon originates from Resonant ν_μ CC interaction then a further cut can be applied. If the muon arising from the event can be identified the event can be removed. As muons are minimum ionising they produce long tracks in the detector. Therefore remove events where the muon travels greater than 1 m it is assumed that the event is a ν_μ CC interaction and the event is removed. In the truth analysis only events where the muon travels greater than one 1 m within the TPC are removed. This cut therefore has no effect on the signal. Figure BLAR shows the efficiency of remove the background as a function of neutrino energy. In a non-truth analysis the muon itself cannot be considered. Figure BLAR shows the reconstructed length of the longest track in the detector for oscillated electrons and ν_μ events with a pizero present in SBND showing a 1 m cut keeps the majority of the events

Events where the shower has an energy less than 200 MeV are removed from the analysis. Figures BLAR, BLAR and BLAR shows the effective of applying this cut on the signal, neutral current background and the charge current background respectively. Figure BLAR shows the actual energy reconstructed of the oscillated Nu_e signal and events ν_μ events with a pizero present in SBND. There is separation in the events of X% efficiency and Y% background rejection. Finally a fiducial volume cut is applied. The fidicial volume cut is tabulated in Figure BLAR and is mainly in effect to remove the dirt background. The dirt background undergoes also undergoes the energy, number of showers cut and dEdx weight. The efficiency of the fiducual volume cut can be seen in Figures BLAR for the Signal, TPC NC Backgrounds and the Dirt Events respectively. A weight of 0.8 is applied to all selected events to account for a 80% reconstruction efficiency. The efficiency of reconstructing neutrino events in the actual reconstruction can be seen in Figure BLAR and BLAR. Figures BLAR and BLAR show the efficiency of the pandora pattern recognition reconstructing a PFP particle for the neutrino for the oscillated electrons and ν_μ events with a pizero present respectively in SBND. This corresponds to global reconstruction efficiency of BLAR however no quality control cuts are considered. Figures BLAR and BLAR show events when more than one PFP particle was reconstructed in the event for oscillated electrons and ν_μ events with a pizero present respectively. There is a significant number of events which are reconstructed more than once. This affect is not considered in the truth based analysis.

The neutrino energy is the reconstructed by summing the depositions of the particles in the event. This includes particles associated to the vertex and the lepton candidate. Both the modern and proposal sample undergo this selection and the spectra for the three detectors are shown in Figures

BLAR to BLAR and Figures BLAR to BlAR respectively.

4.4. Cosmic Removal

For the cosmics a further two cuts are applied. Firstly if the cosmics photon initially interacts outside the Fiducal volume the event is removed. The effectiveness of this cut can be seen in figure BLAR. The beam spill weight described in section BLAR is applied to mimic removing events outside the beam spill window. The dE/dx weight is also applied to the cosmic photons. A weight of 0.05 is also applied to the cosmic events to account for further reductions of cosmics within the beam spill time using the PDG and CRT systems. Finally a cosmic cylinder cut is applied to remove cosmics. Most of the cosmic events occur from as a daughter particle from a through going cosmic muon. A cylinder of 15 cm in radius is applied around every cosmic muon in event, see Figure BLAR. If a cosmic photon background is within the cylinder the event is removed. The effectiveness of the cut can be seen in Figure BLAR.

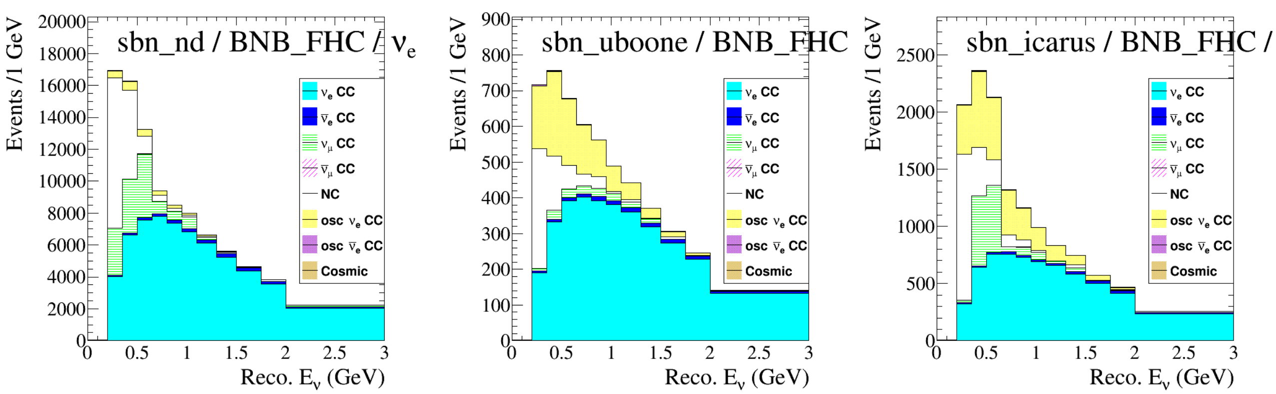

Figure 12: Truth-level Charged Current Muon Neutrino, $\nu_e CC$, interaction rates in the three SBN detectors broken down into the truth-level neutrino interaction mode. From left to right: SBND, MicroBooNE & ICARUS. The Monte Carlo samples used to generate these plots were constructed using the proposal-era procedure. There was no inclusion of MEC in the event rate predictions at this time. The SBN-ND was also positioned at a 100m baseline as opposed to the revised, current 110m baseline.

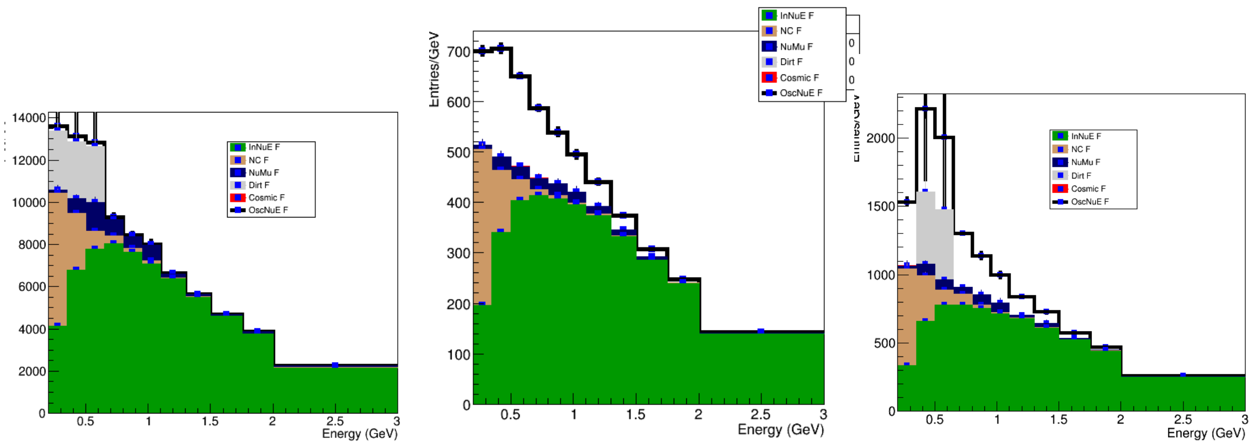

Figure 13: Truth-level Charged Current Muon Neutrino, $\nu_e CC$, interaction rates in the three SBN detectors broken down into the truth-level neutrino interaction mode. From left to right: SBND, MicroBooNE & ICARUS. The Monte Carlo samples used to generate these plots were constructed using the modern-era procedure. The baseline of the SBN-ND is also moved to the correct location at 110m.

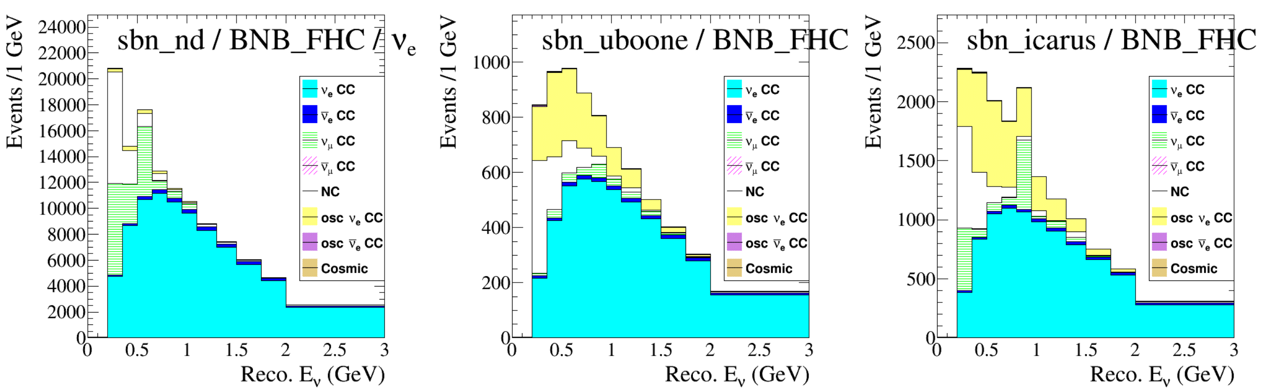

Figure 14: Truth-level Charged Current Muon Neutrino, $\nu_e CC$, interaction rates in the three SBN detectors broken down into the truth-level neutrino interaction mode. From left to right: SBND, MicroBooNE & ICARUS. The Monte Carlo samples used to generate these plots were constructed using the modern-era procedure. The baseline of the SBN-ND is also moved to the correct location at 110m.

5. Systematic Error Assignments

5.1. Flux

Flux Systematics	
expskin_FluxUnisim	Depth that the current penetrates the horn conductor ("skin effect")
horncurrent_FluxUnisim	Current running in the horn conductor
nucleoninexsec_FluxUnisim	Nucleon inelastic cross-section
nucleonqexsec_FluxUnisim	Nucleon quasi-elastic cross-section
nucleontotxsec_FluxUnisim	Nucleon total cross-section
pioninexsec_FluxUnisim	Pion inelastic cross-section
pionqexsec_FluxUnisim	Pion quasi-elastic cross-section
piontotxsec_FluxUnisim	Pion total cross-section

5.2. Neutrino-Nucleus Interactions

Interaction Systematics		
genie_ccresAxial_Genie	Axial mass for CC resonance neutrino production	$\pm$20%
genie_ncresAxial_Genie	Axial mass for NC resonance neutrino production	$\pm$20%
genie_qema_Genie	Axial mass for CC quasi-elastic	-15% +25%
genie_NC_Genie	Axial mass for NC elastic	$\pm$25%
genie_NonResRvbarp1pi_Genie	Non-resonance bkg in νn & $\bar{\nu} p$ CC1π reactions	$\pm$50%
genie_NonResRvbarp2pi_Genie	Non-resonance bkg in νn & $\bar{\nu}$p CC2π reactions	$\pm$50%
genie_NonResRvp1pi_Genie	Non-resonance bkg in νp & $\bar{\nu}$n CC1π reactions	$\pm$50%
genie_NonResRvp2pi_Genie	Non-resonance bkg in νp & $\bar{\nu} n$ CC2π reactions	$\pm$50%
genie_NonResRvbarp1piAlt_Genie	Non-resonance bkg in νn & $\bar{\nu}$p NC1π reactions	$\pm$50%
genie_NonResRvbarp2piAlt_Genie	Non-resonance bkg in νn & $\bar{\nu}$p NC2π reactions	$\pm$50%
genie_NonResRvp1piAlt_Genie	Non-resonance bkg in νp & $\bar{\nu}$n NC1π reactions	$\pm$50%
genie_NonResRvp2piAlt_Genie	Non-resonance bkg in νp & $\bar{\nu}$n NC2π reactions	$\pm$50%

5.3. Detector Response

6. Oscillation Fitting Frameworks

The SBN oscillation analysis paradigm outlined in Sec. 2 was implemented in three independent fitting frameworks: CAFAna (Sec. 6.2), SBNFit (Sec. 6.3) and VALOR (Sec. 6.4). The same MC generated event samples, event selections and systematic error inputs were used in all fitting frameworks. However, the three different frameworks treat systematic inputs slightly differently, and make use of different approximations, as described in the following subsections. As such they provide interesting insights on the impact of these approximations and systematics treatment on the SBN oscillation sensitivity.

6.1. Global Analysis Decisions

In addition to the input central values being identical, the following fitting choices are common to all three fitting frameworks.

The ν_μ binning (edge-to-edge) has 19 bins in reconstructed neutrino energy, defined as xxxx, which are bounded as follows:

- 2 0.1-GeV bins from 0.2-0.4 GeV,
- 12 0.05-GeV bins from 0.4-1.0 GeV,
- 2 0.25-GeV bins from 1.0-1.5 GeV and
- 3 0.5-GeV bins from 1.5-3 GeV.

The ν_e binning (edge-to-edge) has 11 bins in reconstruced neutrino energy, defined as xxxx, which are bounded as follows:

- 6 0.15-GeV bins from 0.2-1.1 GeV,
- 2 0.2-GeV bins from 1.1-1.5 GeV,
- 2 0.25-GeV bins from 1.5-2.0 GeV and
- 1 bin from 2.0-3.0 GeV.

The input spectra are provided in Fig. **??**.

6.2. CAFAna

in progress, adapting text from DUNE CDR

The CAFAna framework was developed for the NOvA experiment and has been used for ν_μ-disappearance, ν_e-appearance, and joint fits, plus sterile neutrino searches and cross-section analyses. CAFAna has now been adapted for use in the DUNE and SBN sensitivity analyses and upcoming NOvA/T2K joint fit.

In the sensitivity studies, the compatibility of a particular oscillation hypothesis with the data is evaluated using the likelihood appropriate for Poisson-distributed data [1]:

$$\chi^2 = -2\log\mathcal{L} = 2\sum_{i}^{N_{\mathrm{bins}}}\left[M_i - D_i + D_i\ln\left(\frac{D_i}{M_i}\right)\right] \tag{1}$$

where M_i is the Monte Carlo expectation in bin i and D_i is the observed count. For these studies the bins here represent reconstructed neutrino energy, but other observables, such as reconstructed kinematic variables or event classification likelihoods may also be used. Multiple samples with different selections can be fit simultaneously, as can multi-dimensional distributions of reconstructed variables.

Event records representing the reconstructed properties of neutrino interactions and, in the case of Monte Carlo, the true neutrino properties are processed to fill the required histograms. Oscillated predictions are created by populating 2D histograms, with the second axis being the true distance travelled divided by neutrino energy, for each oscillation channel ($\nu_\alpha \to \nu_\beta$). These are then reweighted as a function of the true energy axis according to an exact calculation of the oscillation weight at the bin center and summed to yield the total oscillated prediction:

$$M_i = \sum_{\alpha}^{e,\mu} \sum_{\beta}^{e,\mu,\tau} \sum_{j} P_{\alpha\beta}(E_j) M_{ij}^{\alpha\beta} \tag{2}$$

where $P_{\alpha\beta}(E)$ is the probability for a neutrino created in flavor state α to be found in flavor state β at the desired baseline. $M_{ij}^{\alpha\beta}$ represents the number of selected events in bin i of the reconstructed variable with true L_j/E_j, taken from a simulation where neutrinos of flavor α from the beam have been replaced by equivalent neutrinos in flavor β. Various oscillation calculations are available, *e.g.* three-flavor oscillations with matter effects or full four-flavor sterile oscillations. For this study oscillation probabilities are calculated in the 3+1 sterile neutrino model using a two-flavor approximation. The oscillation probabilities for beam ν_μ are

$$\begin{aligned}
P(\nu_\mu \to \nu_\mu) &= 1 - \sin^2 2\theta_{\mu\mu} \sin^2\left(\frac{1.267\Delta m^2 L}{E}\right) && (3)\\
P(\nu_\mu \to \nu_e) &= \sin^2 2\theta_{\mu e} \sin^2\left(\frac{1.267\Delta m^2 L}{E}\right) && (4)\\
P(\nu_\mu \to \nu_s) &= \left(\sin^2 2\theta_{\mu\mu} - \sin^2 2\theta_{\mu e}\right) \sin^2\left(\frac{1.267\Delta m^2 L}{E}\right) && (5)
\end{aligned}$$

with similar expressions for the oscillations of intrinsic beam ν_e. In order to treat the rapid-oscillation regime, the oscillation probability is averaged analytically over the true energy bin.

Systematic uncertainties are included to account for the expected uncertainties in the beam flux, neutrino interaction, and detector response models used in the simulation at the time of the analysis. The impact of systematic uncertainties is included by adding additional nuisance parameters into the fit. Each of these parameters can have arbitrary effects on the Monte Carlo prediction, and can affect the various samples and channels within each sample in different ways. These parameters are profiled over in the production of the result. The range of these parameters is controlled by the use of Gaussian penalty terms to reflect our prior knowledge of reasonable variations.

For each systematic parameter under consideration, the matrices $M_{ij}^{\alpha\beta}$ are evaluated for a range of values of the parameter, by default $\pm 1, 2, 3\sigma$. The predicted spectrum at any combination of systematic parameters can then be found by interpolation. Cubic interpolation is used, which guarantees continuous and twice-differentiable results, advantageous for gradient-based fitters such as MINUIT. The SBN analysis files treat systematic uncertainties with a "multiverse" approach. For each randomly thrown systematic universe the value taken by each systematic parameter, and the corresponding factor in the overall event weight are stored. This allows CAFAna to identify universes where a specific parameter takes desired values, and isolate the effect of that single parameter in order to fill the required matrices.

6.3. SBNFit

6.3.1. Introduction

In Progress The SBNfit framework is a spiritual successor to the general fitting approach that has been followed in MiniBooNE and was developed for an independent phenomenological study of Fermilab's short-baseline program [**?**]. It has since been generalized, extended and adopted by the MicroBooNE collaboration as the primary fitting tool. The SBNfit framework [**?**] provides capability of 3+N sterile neutrino oscillation combined fits with arbitrary numbers of detectors. It utilizes a simultaneous, side-by-side fit of multiple event samples by way of a full covariance matrix that contains the full statistical and systematic uncertainties as well as systematic correlations among the different samples (and across different detectors).

The test statistic as utilized by SBNfit is a χ^2 calculated over the concatenated ν_e CC inclusive and/or ν_μ CC inclusive spectra for all three detectors, defined as

$$\chi^2(\Delta m^2_{i1}, U_{\alpha i}) = \sum_{k=1}^{M}\sum_{l=1}^{M}\left[D_k - P_k^{osc}(\Delta m^2_{i1}, U_{\alpha i})\right] E^{-1}_{kl}\left[D_l - P_l^{osc}(\Delta m^2_{i1}, U_{\alpha i})\right] , \tag{6}$$

where D_k is some real or hypothetical (or fake) number of data events in the k^{th} bin of reconstructed neutrino energy; $P_k^{osc}(\Delta m^2_{i1}, U_{\alpha i})$ is the number of signal and background events predicted to be observed in reconstructed neutrino energy bin k under an oscillation hypothesis described by the set of parameter values $(\Delta m^2_{i1}, U_{\alpha i})$; and E_{kl} is a full $M \times M$ covariance matrix containing the total systematic and statistical uncertainty squared, including systematic correlations between any two bins k and l. (Details of the covariance matrix construction are provided below).

When working with vacuum oscillation probabilities, or in the short-baseline approximation, where matter effects can safely be ignored, all neutrino appearance and disappearance oscillation probabilities for any arbitrary number of additional sterile neutrinos can be re-written in the representative form:

$$P^{3+N}_{\nu_\alpha\to\nu_\beta}(E_\nu, L_{osc}, \Delta m^2_{i1}, U_{\alpha i}) = \sum A(U_{\alpha i})\sin^2\left(\frac{\Delta m^2_{i1}L_{osc}}{4E_\nu}\right) + \sum B(U_{\alpha i})\sin\left(\frac{\Delta m^2_{i1}L_{osc}}{2E_\nu}\right) \tag{7}$$

i.e., as a sum of sin and $\sin^2$ frequencies, which are functions of energy and baseline, scaled by amplitudes (A,B) which are functions of the mixing elements only. SBNfit takes advantage of this simplification to pre-calculate the individual sin and $\sin^2$ frequency spectra for any given mass-splittings and then at run time during fitting, any complete oscillated spectra can be found by merely adding and scaling by the appropriate amplitudes. As the frequency templates are constructed directly from oscillating the MC event-by-event, the true true energy and true baseline is user per event, with no approximation or binning in true energy/baseline needed. Although even in the case of arbitrary matter potentials, one can always rewrite the oscillation probabilities in this form, for non-zero matter potentials the amplitudes become a function of Δm^2 and L_{osc} and thus the templating of frequencies no longer works.

6.3.2. Construction of Covariance Matrix

All systematics and information on their correlations is included via the combined covariance matrix. At the moment this is restrited to just flux and interaction/cross-section uncertainties that are estimated via reweighting the Monte Carlo CV. The reweighting of the CV for flux and cross-section systematics is stored in the eventweight class. This eventweight class in SBNcode is defined as a `std::map<std::string,std::vector<float>>`, and SBNfit utilizes the same structure for maximum compatibility and convenience. The strings are a unique tag that defines the variation, e.g GENIE CCQE MA, or Sandford-Wang flux variations , and the `vector<float> is the series of N weights, were N`

$$E^v_{i,j} = \frac{1}{N^v} \sum_k^{N^v} (P_i^{CV} - P_i^k) * (P_j^{CV} - P_j^k) \tag{8}$$

The total covariance matrix is then the linear sum of all individual flux and cross-section covariance matrices;

$$E^{tot}_{i,j} = \sum_{flux} E^v_{i,j} + \sum_{interaction} E^v_{i,j} \tag{9}$$

Note that the number of universes that each variation is associated with, N^v, do not have to be the same and variations for which more of an effect is expected can have more universes to ensure good coverage.

The calculated covariance matrix is computed breaking down each catagory into its subcomponents, e.g CC ν_e inclusive has components coming from intrinsic ν_e, oscillated ν_μ, ν_μ mis-id ..etc.. making it significantly larger than the final covariance matrix used in the fit. Having the full covariance matrix with each component split out allows the effects of particular correlations to be highlighted, as well as allows for the oscillation of various subcomponents separately. To go from the full covaraince to the smaller physical version used in the fits, we collapse by matrix adding each of the subchannel blocks of the full covariance down to a single channel . Bit more description needed, add example correlation matrix.

6.3.3. SBN Proposal and Modern sensitivity calculations specifics

When oscillating the true baseline was calculated on a event-by-event basis using the true neutrino information, via the SBNreco TTree's variable "truth.neutrino.baseline". For the "proposal" datasets, however, although the 10m shift in SBND location was taken into account for rates, the baseline was not changed in the truth.neutrino.baseline variable and so a manual 10m shift is included when oscillating. There is also an additional event-by-event reco.weight applied per event.

Included in analysis is 20 systematic uncertainties. Of these 8 are flux uncertainties:

`expskin_FluxUnisim, horncurrent_FluxUnisim, nucleoninexsec_FluxUnisim, nucleonqexsec_FluxUnisim, pioninexsec_FluxUnisim, nucleontotxsec_FluxUnisim, pionqexsec_FluxUnisim and piontotxsec_FluxUnisim`

The remaining 12 are interaction uncertainties;

`ccresAxial, ncresAxial, qema, NC, NonResRvbarp1pi, NonResRvbarp2pi, NonResRvp1pi, _NonResRvp2pi, NonResRvbarp1piAlt, NonResRvbarp2piAlt,  NonResRvp1piAlt and NonResRvp2piAlt`

At the moment 5 systematics that were included in the proposal are not included in order to facilitate a more direct comparison between SBNfit and CAFAna/VALOR. The 5 are all flux uncertainties:

`kminus_PrimaryHadronNormalization, kplus_PrimaryHadronFeynmanScaling, kzero_PrimaryHadronSanfordWang, piminus_PrimaryHadronSWCentralSplineVariation and piplus_PrimaryHadronSWCentralSplineVariation.`

It is worth noting that in particular, `piplus_PrimaryHadronSWCentralSplineVariation`, is known to have a large effect on the low Δm^2 region.

6.4. VALOR

6.4.1. Introduction

VALOR[1] is a modern oscillation analysis framework, that was first established within the T2K experiment in 2010 and named after its initial participants (VALencia-Oxford-Rutherford), a name that was maintained although the group has since expanded substantially. Since 2010, the VALOR group performed around 20 iterations of T2K electron-(anti)neutrino appearance, muon-(anti)neutrino disappearance, and joint 3-flavour analyses and it

[1]https://valor.pp.rl.ac.uk

contributed to nearly all published T2K oscillation results. 2019 saw the completion of a large-scale code refactoring, painstakingly carving a generic, CPU efficient and highly flexible oscillation analysis *framework*, the VALOR Software Development Kit (VALOR SDK), out of a leading 3-flavour oscillation analysis. The development of the VALOR SDK has streamlined use of VALOR in several experimental setups without the need to maintain multiple separate forks: Currently several distinct oscillation analyses (T2K, SuperK atmospherics, joint T2K+SuperK, joint T2K+NOvA, DUNE, SBN) are (or are being) built as a thin layer of experiment-specific definitions and data inputs on top of that single VALOR SDK. A VALOR adaptation for the SBN, implementing at first the same analysis paradigm as the one used for the SBN proposal, was completed in 2019. The following subsections give a brief overview of VALOR SDK, and of the tools used to construct the SBN physics parameterization and interpret SBN data.

6.4.2. Framework for construction of physics parameterization

In the VALOR SDK an arbitrary number of samples, each corresponding to a given i) detector (or sub-detector region), ii) beam configuration, iii) observed final state, and iv) kinematic phase space, can be fit jointly to determine the parameters of a physics hypothesis in the presence of uncertainties.

A crucial element of parameter and error estimation in the context of an oscillation analysis is the efficient calculation of event rate predictions, both nominal and varied ones corresponding to specific combination of systematic effects and oscillation (or other new physics) hypotheses. Event rate predictions needs to be calculated for each topological event sample included in the fit, as a function of the observed kinematic quantities chosen for each sample. Predictions are constructed from Monte Carlo (MC) templates T, which represent the number of MC events (after event selection cuts were applied on the output of the full event simulation and reconstruction chain) as function of several reconstructed and true quantities, as needed in order to apply physics and systematic effects as function of the most appropriate variables, and in order to enable comparisons with the chosen observed kinematic distributions. Separate MC templates are constructed for each detector d, beam configuration b, and sample s. Each MC template contains information on how the number of events is distributed in the same N_r-dimensional space K_r of reconstructed kinematic variables chosen for the fit samples. The same reconstructed kinematic variable binning scheme is used both for the

MC templates and the fit distributions. The MC templates provide a mapping between reconstructed and true information. Separate templates are constructed for different true reaction modes m, and each template contains information on how the number of events, for each individual reconstructed bin, is distributed in a chosen N_t-dimensional space K_t of true kinematic variables. The true reaction modes, the true kinematic variables, and the kinematic variable binning schemes are defined so that the intended flavour dependencies, reaction mode dependencies and kinematic dependencies of systematics and/or of considered physics hypotheses can be taken into account. Therefore, summarizing all MC template dependencies, we can write

$$T = T_{d;b;s;m}(r, t) \tag{10}$$

where r is a bin in the K_r space of reconstructed kinematic variables, and t is a bin in the K_t space of true kinematic variables. A MC template $T_{d;b;s;m}$ is constructed from a MC sample corresponding to an exposure of $e^{MC}_{d;b}$ and then used to predict observations, or fit data, corresponding to an exposure of $e^{data}_{d;b}$. Here, we will assume that a scaling factor $e^{data}_{d;b}$ / $e^{MC}_{d;b}$ is absorbed in the definition of $T_{d;b;s;m}$.

Using MC templates, the predicted number of events $n^{pred}_{d;b;s}(r;\vec{\theta};\vec{f})$ in a N_r-dimensional reconstructed kinematic bin r, for a specific sample s, seen in a detector d exposed in a beam configuration b, and for a particular set of M physics parameters $\vec{\theta} = (\theta_0, \theta_1, ..., \theta_{M-1})$ and N nuisance (systematic) parameters $\vec{f} = (f_0, f_1, ..., f_{N-1})$, is computed as

$$n^{pred}_{d;b;s}(r;\vec{\theta};\vec{f}) = \sum_m \sum_t P_{d;b;m}(t;\vec{\theta}) \cdot R_{d;b;s;m}(r, t;\vec{f}) \cdot T_{d;b;s;m}(r, t) \tag{11}$$

where $P_{d;b;m}(t;\vec{\theta})$ encapsulates the effect of a physics hypothesis (e.g. neutrino oscillations in a 3-flavour framework), and $R_{d;b;s;m}(r, t;\vec{f})$ parameterizes the response of a template bin to systematic variations. In principle, the range of m values in the above sum depends on the sample s. In addition, the number, type and dimensionality of true bins t is a function of both s and m. The above will be assumed implicitly and not written explicitly.

The term $P_{d;b;m}(t;\vec{\theta})$ is naturally only a function of true kinematic variables and of neutrino flavour and/or true reaction mode (both of which are encapsulated in m). For multi-detector fits, the dependence on d and b reflects the dependence of P on the appropriate baseline (or on the distribution of baselines in SBL oscillation variants of the VALOR analysis). The oscillation probability $P_{d;b;m}(t;\vec{\theta})$ is evaluated in one of a number of different physics frameworks, each with its own set of parameters $\vec{\theta}$. Currently, the VALOR SDK supports oscillation probability calculations in a 3-flavour framework, as well as 3+1 and 3+2 frameworks, considering matter-effects in constant density matter and, optionally, non-standard interactions. In addition, simpler 2-flavour oscillation probability calculations are also supported. The application of the term $P_{d;b;m}(t;\vec{\theta})$ requires some extra elaboration as it is likely to lead to conceptual oddities when joint, multi-channel analyses are performed within simplified, effective 2-flavour frameworks (as it is the case for this round of SBN oscillation sensitivity calculations). In general, in a 3-flavour analysis, the CC MC templates constructed from the unoscillated MC samples are weighted with the corresponding survival probability: The ν_μ CC templates are weighted with $P(\nu_\mu \rightarrow \nu_\mu)$, the $\bar{\nu}_\mu$ CC templates are weighted with $P(\bar{\nu}_\mu \rightarrow \bar{\nu}_\mu)$, the ν_e CC templates are weighted with $P(\nu_e \rightarrow \nu_e)$, and the $\bar{\nu}_e$ CC templates are weighted with $P(\bar{\nu}_e \rightarrow \bar{\nu}_e)$, The CC MC templates made from the *oscillated (or swapped)* ν_e event sample (a ν_e event sample that was generated with the ν_μ flux, as if all ν_μ's converted to ν_e) are weighted with $P(\nu_\mu \rightarrow \nu_e)$. Similarly, if there was any, CC MC templates made from an *oscillated* $\bar{\nu}_e$ event sample would be weighted with $P(\bar{\nu}_\mu \rightarrow \bar{\nu}_e)$, CC MC templates made from an *oscillated* ν_μ event sample would be weighted with $P(\nu_e \rightarrow \nu_\mu)$, and CC MC templates made from an *oscillated* $\bar{\nu}_\mu$ event sample would be weighted with $P(\bar{\nu}_e \rightarrow \bar{\nu}_\mu)$. Contributions from ν_τ CC and $\bar{nu}_\tau$ CC are neglected as, even when they are produced via oscillations, have a negligible effect on observed distributions due to the high energy threshold for τ production. The same oscillation parameters are used for both neutrino and anti-neutrino oscillations. Oscillations are not applied to the NC MC templates since, effectively, they serve as proxies for the mixtures of $\nu_e + \nu_\mu + \nu_\tau$ NC and $\bar{\nu}_e + \bar{\nu}_\mu + \bar{\nu}_\tau$ MC templates which are unchanged under 3-flavour oscillations. How this general scheme is modified within the *effective* 3+1 framework used for this round of SBN sensitivity calculations is summarised in Sec. 6.4.4.

Typically, but not always, the response $R_{d;b;s;m}(r,t;\vec{f})$ factorises and it can be written as

$$R_{d;b;s;m}(r,t;\vec{f}) = \prod_{i=0}^{N-1} R^i_{d;b;s;m}(r,t;f_i) \tag{12}$$

For several systematics the response is linear and, therefore,

$$R^i_{d;b;s;m}(r,t;f_i) \propto f_i \tag{13}$$

For non-linear systematics, the response function $R^i_{d;b;s;m}(r,t;f_i)$ is usually pre-computed in the [-5σ, +5σ] range of the parameter f_i and it is represented internally using Akima or cubic splines. Values of systematic parameters that give a negative predicted number of events in any reconstructed bin in any interaction mode are not allowed.

Once the construction of predictions $n^{pred}_{d;b;s}(r;\vec{\theta};\vec{f})$ is possible within VALOR, through the factorization described in Eq. 11, physics is extracted through a comparison with observed (or simulated fake) data, which are denoted as $n^{obs}_{d;b;s}(r)$ and represent the observed event rate for each detector d, beam configuration b, topological sample s and (multi-dimensional) reconstructed kinematic bin r. VALOR, typically, uses a binned likelihood ratio method and, therefore, attempts to minimize the quantity:

$$-2ln\lambda(\vec{\theta};\vec{f}) = 2\sum_{d,b,s,r}\Big(n^{obs}_{d;b;s}(r)\cdot ln\frac{n^{obs}_{d;b;s}(r)}{n^{pred}_{d;b;s}(r;\vec{\theta};\vec{f})} + (n^{pred}_{d;b;s}(r;\vec{\theta};\vec{f}) - n^{obs}_{d;b;s}(r))\Big) - 2ln\lambda_{penalty}(\vec{\theta};\vec{f}) \tag{14}$$

where $-2ln\lambda_{penalty}$ is a penalty term encapsulating prior constraints from non-SBN data. The advantage of the likelihood ratio method, compared with the extended maximum-likelihood method, is that in the large-sample limit, the quantity $-2ln\lambda(\vec{\theta};\vec{f})$ has a χ^2 distribution and it can therefore be used as a goodness-of-fit test. Various strategies are employed for the minimisation of $-2ln\lambda(\vec{\theta};\vec{f})$, the elimination of nuisance and/or interesting physics parameters, and the construction of confidence intervals. These statistical procedures implemented within the VALOR SDK are summarised in Sec. 6.4.3.

The calculation of $-2ln\lambda(\vec{\theta};\vec{f})$ outlined above encapsulates the VALOR *physics parameterization*, i.e. It is clear, that the above is simply an efficient computational framework for an analysis and not an analysis in itself. It allows a number of analysis-specific choices to be made, and different choices are appropriate for different detector technologies, energy ranges, systematic error regimes and physics hypotheses under investigation. These analysis-specific choices include:

- The definition of topological event samples s. In principle, these samples can be different for different detectors allowing, for example, the higher statistics SBND samples to be further subdivided into several exclusive channels and utilise correlations in order to disentangle systematic effects.

- The definition of reconstructed and true kinematic spaces. This includes the choice of kinematic space dimensionalities, the choice of kinematic quantities, and the choice of binning schemes (fixed and variable width binning schemes, both edge-to-edge and *Mondrian* type ones are supported within the VALOR SDK). In principle, the choice of a reconstructed kinematic space can be unique to each topological sample included in the fit.

- The choice of generator-level labels (modes m), whose contributions to the predicted event rate for a given topological sample are individually tracked. This choice can be unique to each topological sample included in the fit and it is crucial (along with the choice of kinematic quantities) so that the application of systematic and physics effects can be finally targeted and expressed with the most natural degrees of freedom.

- The choice of systematic parameters, the parameterization of the effect of systematic parameters on the computed event rates, and the definition of prior systematic parameter constraints.

All the above are very flexibly defined within with the VALOR SDK. Choices specific to the current round of SBN oscillation sensitivity calculations (2019b) are outlined in Sec. 6.4.4.

6.4.3. Fitting, elimination of nuisance parameters and construction of confidence intervals

6.4.4. Choices specific to the current SBN sensitivity calculations

The ν_μ reaction modes used are:

- ν_μ CC QE
- ν_μ CC MEC
- ν_μ CC $1\pi^\pm$
- ν_μ CC $2\pi^\pm$
- ν_μ CC other

- $\bar{\nu}_\mu$ CC
- $\nu_e/\bar{\nu}_e$ CC
- NC
- Cosmic

The ν_e reaction modes used are:

- ν_e CC
- $\bar{\nu}_e$ CC
- ν_μ CC
- $\bar{\nu}_\mu$ CC
- NC
- osc ν_e CC
- osc $\bar{\nu}_e$ CC
- Cosmic

The ν_μ binning (edge-to-edge) has 33 true bins which are arranged as follows:

- 2 0.25-GeV bins from 0-0.5 GeV,
- 15 0.05-GeV bins from 0.5-1.25 GeV,
- 15 0.25-GeV bins from 1.25-5.0 GeV and
- 1 bin from 5.0-10.0 GeV.

The ν_e binning (edge-to-edge) has 33 true bins which are the same as the ν_μ ones.

Correlated flux and interaction systematic uncertainties		
Parameter	Description	1σ frac. error

	ν_μ disappearance SBND flux parameters	
0	$E_{\nu,Reco}$ = 0.2-0.3 GeV	0.0636
1	$E_{\nu,Reco}$ = 0.3-0.4 GeV	0.0543
2	$E_{\nu,Reco}$ = 0.4-0.45 GeV	0.0516
3	$E_{\nu,Reco}$ = 0.45-0.5 GeV	0.0500
4	$E_{\nu,Reco}$ = 0.5-0.55 GeV	0.0490
5	$E_{\nu,Reco}$ = 0.55-0.6 GeV	0.0486
6	$E_{\nu,Reco}$ = 0.6-0.65 GeV	0.0485
7	$E_{\nu,Reco}$ = 0.65-0.7 GeV	0.0489
8	$E_{\nu,Reco}$ = 0.7-0.75 GeV	0.0502
9	$E_{\nu,Reco}$ = 0.75-0.8 GeV	0.0515
10	$E_{\nu,Reco}$ = 0.8-0.85 GeV	0.0534
11	$E_{\nu,Reco}$ = 0.85-0.9 GeV	0.0557
12	$E_{\nu,Reco}$ = 0.9-0.95 GeV	0.0589
13	$E_{\nu,Reco}$ = 0.95-1.0 GeV	0.0628
14	$E_{\nu,Reco}$ = 1.0-1.25 GeV	0.0763
15	$E_{\nu,Reco}$ = 1.25-1.5 GeV	0.111
16	$E_{\nu,Reco}$ = 1.5-2.0 GeV	0.154
17	$E_{\nu,Reco}$ = 2.0-2.5 GeV	0.140
18	$E_{\nu,Reco}$ = 2.5-3.0 GeV	0.0800
	ν_μ disappearance MicroBooNE flux parameters	
19	$E_{\nu,Reco}$ = 0.2-0.3 GeV	0.0675
20	$E_{\nu,Reco}$ = 0.3-0.4 GeV	0.0605
21	$E_{\nu,Reco}$ = 0.4-0.45 GeV	0.0568

22	$\mathrm{E}_{\nu,Reco}$ = 0.45-0.5 GeV	0.0550
23	$\mathrm{E}_{\nu,Reco}$ = 0.5-0.55 GeV	0.0536
24	$\mathrm{E}_{\nu,Reco}$ = 0.55-0.6 GeV	0.0528
25	$\mathrm{E}_{\nu,Reco}$ = 0.6-0.65 GeV	0.0522
26	$\mathrm{E}_{\nu,Reco}$ = 0.65-0.7 GeV	0.0525
27	$\mathrm{E}_{\nu,Reco}$ = 0.7-0.75 GeV	0.0531
28	$\mathrm{E}_{\nu,Reco}$ = 0.75-0.8 GeV	0.0540
29	$\mathrm{E}_{\nu,Reco}$ = 0.8-0.85 GeV	0.0562
30	$\mathrm{E}_{\nu,Reco}$ = 0.85-0.9 GeV	0.0582
31	$\mathrm{E}_{\nu,Reco}$ = 0.9-0.95 GeV	0.0607
32	$\mathrm{E}_{\nu,Reco}$ = 0.95-1.0 GeV	0.0646
33	$\mathrm{E}_{\nu,Reco}$ = 1.0-1.25 GeV	0.0769
34	$\mathrm{E}_{\nu,Reco}$ = 1.25-1.5 GeV	0.108
35	$\mathrm{E}_{\nu,Reco}$ = 1.5-2.0 GeV	0.148
36	$\mathrm{E}_{\nu,Reco}$ = 2.0-2.5 GeV	0.136
37	$\mathrm{E}_{\nu,Reco}$ = 2.5-3.0 GeV	0.0798
	ν_μ disappearance ICARUS flux parameters	
38	$\mathrm{E}_{\nu,Reco}$ = 0.2-0.3 GeV	0.0669
39	$\mathrm{E}_{\nu,Reco}$ = 0.3-0.4 GeV	0.0600
40	$\mathrm{E}_{\nu,Reco}$ = 0.4-0.45 GeV	0.0567
41	$\mathrm{E}_{\nu,Reco}$ = 0.45-0.5 GeV	0.0556
42	$\mathrm{E}_{\nu,Reco}$ = 0.5-0.55 GeV	0.0541
43	$\mathrm{E}_{\nu,Reco}$ = 0.55-0.6 GeV	0.0537
44	$\mathrm{E}_{\nu,Reco}$ = 0.6-0.65 GeV	0.0529
45	$\mathrm{E}_{\nu,Reco}$ = 0.65-0.7 GeV	0.0536

46	$E_{\nu,Reco}$ = 0.7-0.75 GeV	0.0542
47	$E_{\nu,Reco}$ = 0.75-0.8 GeV	0.0553
48	$E_{\nu,Reco}$ = 0.8-0.85 GeV	0.0574
49	$E_{\nu,Reco}$ = 0.85-0.9 GeV	0.0592
50	$E_{\nu,Reco}$ = 0.9-0.95 GeV	0.0633
51	$E_{\nu,Reco}$ = 0.95-1.0 GeV	0.0653
52	$E_{\nu,Reco}$ = 1.0-1.25 GeV	0.0805
53	$E_{\nu,Reco}$ = 1.25-1.5 GeV	0.115
54	$E_{\nu,Reco}$ = 1.5-2.0 GeV	0.158
55	$E_{\nu,Reco}$ = 2.0-2.5 GeV	0.146
56	$E_{\nu,Reco}$ = 2.5-3.0 GeV	0.0866
	ν_μ disappearance interaction parameters	
57	$E_{\nu,Reco}$ = 0.2-0.3 GeV	0.0744
58	$E_{\nu,Reco}$ = 0.3-0.4 GeV	0.0822
59	$E_{\nu,Reco}$ = 0.4-0.45 GeV	0.0870
60	$E_{\nu,Reco}$ = 0.45-0.5 GeV	0.0905
61	$E_{\nu,Reco}$ = 0.5-0.55 GeV	0.0889
62	$E_{\nu,Reco}$ = 0.55-0.6 GeV	0.0886
63	$E_{\nu,Reco}$ = 0.6-0.65 GeV	0.0887
64	$E_{\nu,Reco}$ = 0.65-0.7 GeV	0.0903
65	$E_{\nu,Reco}$ = 0.7-0.75 GeV	0.0921
66	$E_{\nu,Reco}$ = 0.75-0.8 GeV	0.0924
67	$E_{\nu,Reco}$ = 0.8-0.85 GeV	0.0948
68	$E_{\nu,Reco}$ = 0.85-0.9 GeV	0.0967
69	$E_{\nu,Reco}$ = 0.9-0.95 GeV	0.0967

70	$E_{\nu,Reco}$ = 0.95-1.0 GeV	0.0973
71	$E_{\nu,Reco}$ = 1.0-1.25 GeV	0.0978
72	$E_{\nu,Reco}$ = 1.25-1.5 GeV	0.100
73	$E_{\nu,Reco}$ = 1.5-2.0 GeV	0.101
74	$E_{\nu,Reco}$ = 2.0-2.5 GeV	0.100
75	$E_{\nu,Reco}$ = 2.5-3.0 GeV	0.100

Table 5: The fractional, 1σ uncertainty due to prior constraints on each flux and interaction systematic parameter. The flux parameters are divided into contributions from each of the detectors in the SBN program. The basis of these parameters has been translated from those described in Tables 5.1 & 5.2 into a normalisation per $E_{\nu,Reco}$ bin for use by VALOR in the SBN analysis. These parameters are depicted graphically in Figure 20.

Baseline approximation: Each neutrino event has an associated energy and baseline. Within the VALOR framework, events are binned in energy and then oscillations are calculated on a per bin basis. Using the true baseline for each event therefore doesn't line up with the method used by VALOR. To try and emulate the true neutrino baseline for each event, a *variable baseline* was implemented, which is a spline approximating the true neutrino baseline for each detector. The spline allows the baseline distribution to be extracted so when the oscillation probability is calculated it is done N times along the distribution instead of once at the mean baseline.

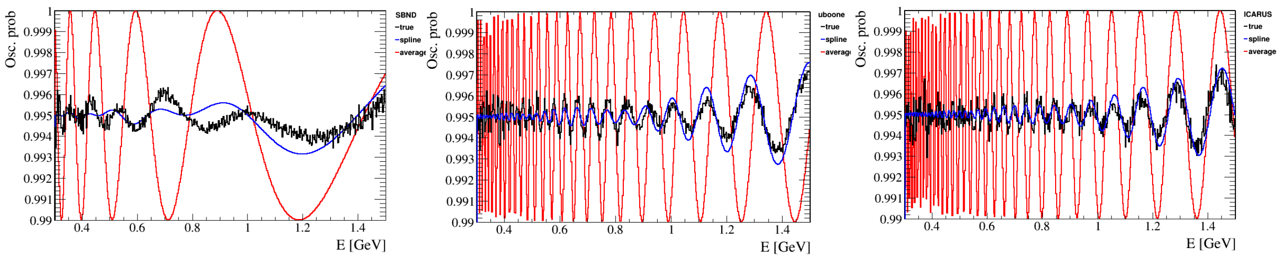

Figure 15: Oscillation probability for each of the the three SBN detectors (from left to right: SBND, MicroBooNe & ICARUS). Oscillation probabilities are calculated for the average baseline (red), the variable baseline (blue) and the true baseline (black) using the parameters $\Delta m^2_{41} = 50$ eV^2 and $sin^2 2\theta_{\mu\mu} = 0.01$. The variable baseline is a spline approximating the true baseline distribution for a given detector.

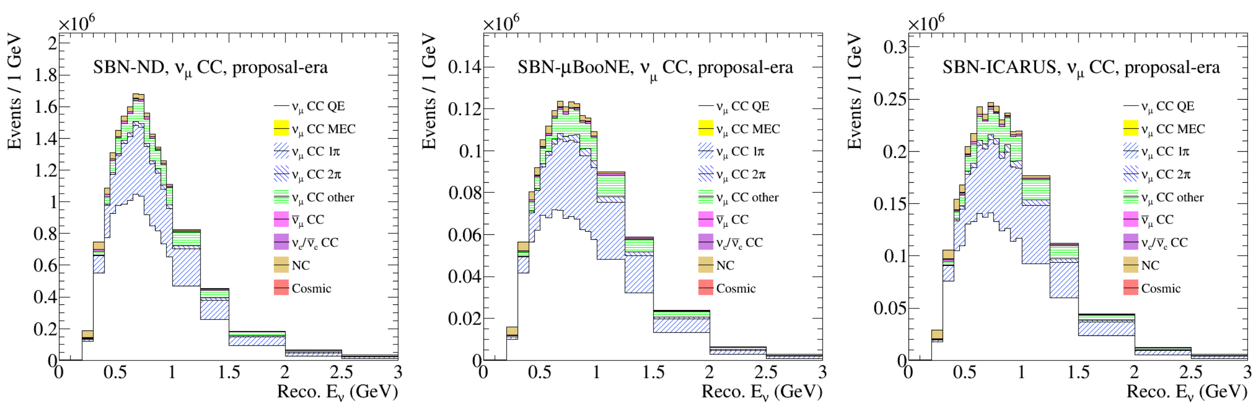

Figure 16: Truth-level Charged Current Muon Neutrino, $\nu_\mu CC$, interaction rates in the three SBN detectors broken down into the truth-level neutrino interaction mode. From left to right: SBND, MicroBooNE & ICARUS. The Monte Carlo samples used to generate these plots were constructed using the proposal-era procedure. There was no inclusion of MEC in the event rate predictions at this time. The SBN-ND was also positioned at a 100m baseline as opposed to the revised, current 110m baseline.

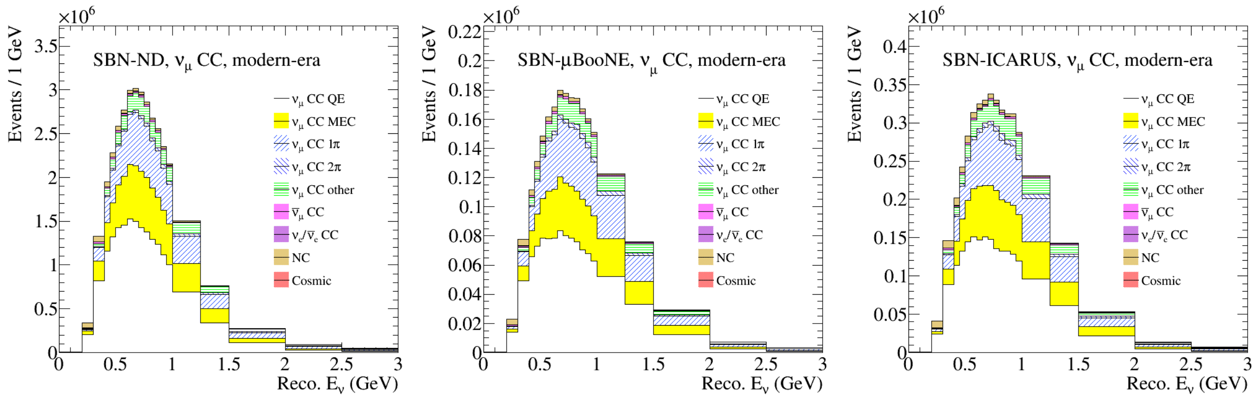

Figure 17: Truth-level Charged Current Muon Neutrino, $\nu_\mu CC$, interaction rates in the three SBN detectors broken down into the truth-level neutrino interaction mode. From left to right: SBND, MicroBooNE & ICARUS. The Monte Carlo samples used to generate these plots were constructed using the modern-era procedure. The baseline of the SBN-ND is also moved to the correct location at 110m.

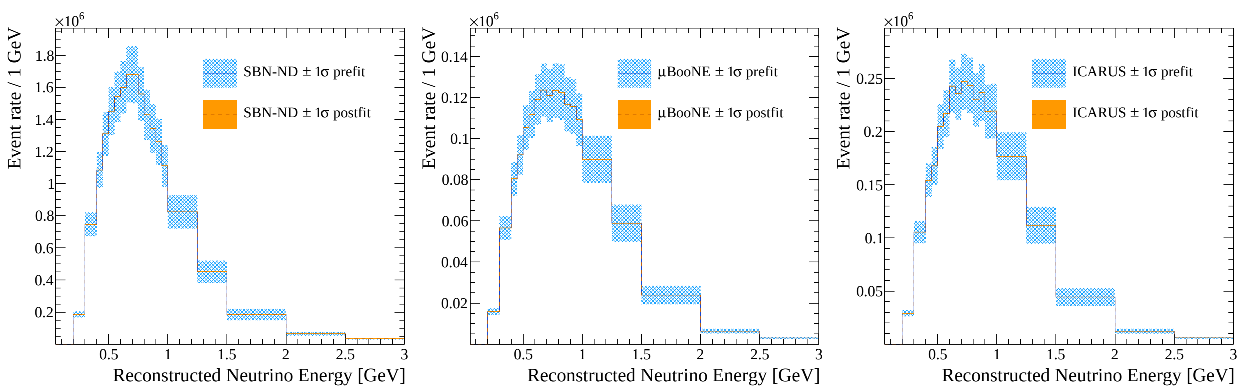

Figure 18: Truth-level Charged Current Muon Neutrino, $\nu_\mu CC$, integrated event rates in the three SBN detectors with a 1σ systematic error band from before and after the three-detector fit under the 3+1 sterile hypothesis between the MC and a toy prediction was performed. From left to right: SBND, MicroBooNE & ICARUS. The Monte Carlo samples used to generate these plots were constructed using the proposal-era procedure. The SBN-ND was also positioned at a 100m baseline as opposed to the revised, current 110m baseline.

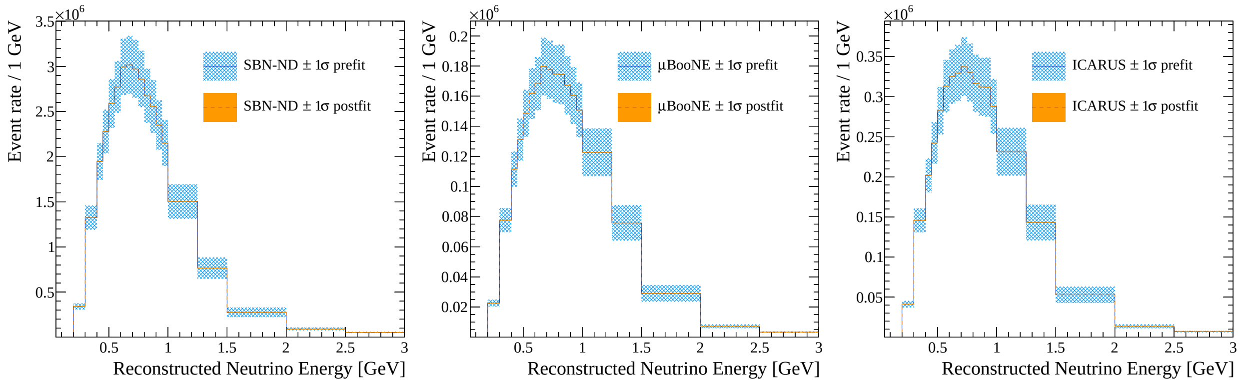

Figure 19: Truth-level Charged Current Muon Neutrino, $\nu_\mu CC$, integrated event rates in the three SBN detectors with a 1σ systematic error band from before and after the three-detector fit under the 3+1 sterile hypothesis between the MC and a toy prediction was performed. From left to right: SBND, MicroBooNE & ICARUS. The Monte Carlo samples used to generate these plots were constructed using the using the modern-era procedure.

7. Oscillation Sensitivity Calculations and Discussion

7.1. Muon-neutrino disappearance

7.1.1. Event rates in the SBN program

7.1.2. Characteristics of the systematic uncertainties in VALOR

7.1.3. Oscillation sensitivities

7.2. Electron-neutrino appearance

8. Summary

Appendix A. Code availability

References

[1] M. Tanabashi, et al. (Particle Data Group), Review of Particle Physics, Phys. Rev. D98 (2018) 030001. doi:10.1103/PhysRevD.98.030001.

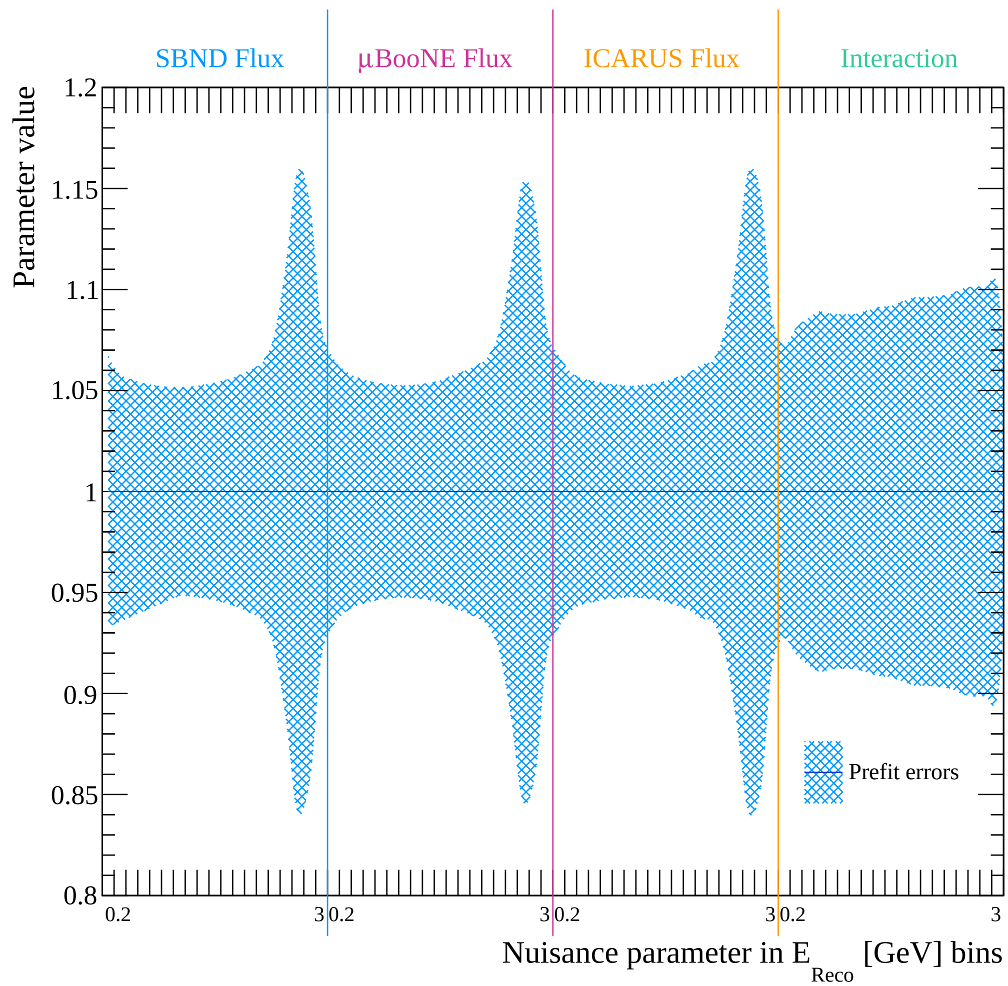

Figure 20: The prior uncertainties on the nuisance parameters defined in Table 5. The prior uncertainties were taken directly from the input covariance matrix generated by the VALOR fitting framework. The SBND flux parameter uncertainties are in the left 19 bins, μBooNE flux in the following 19 bins, ICARUS flux to the right of μBooNE and finally the interaction parameter uncertainties are displayed in the right-most 19 bins. These interaction uncertainties are identical for every experiment in the SBN program.

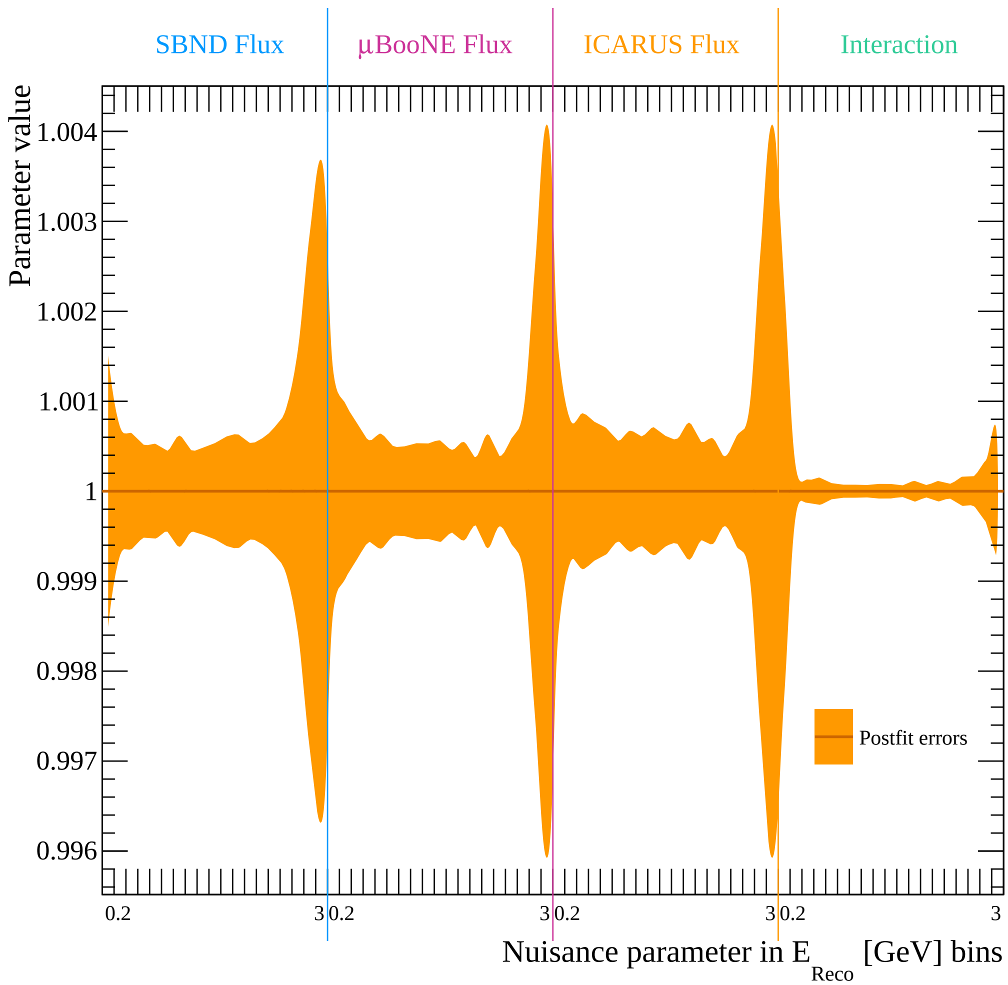

Figure 21: The postfit uncertainties on the nuisance parameters defined in Table 5. The postfit uncertaintes are the result of a fit between the MC and a toy prediction generated using the same MC sample, consequently they have been highly constrained and are very small. The SBND flux parameter uncertainties are in the left 19 bins, μBooNE flux in the following 19 bins, ICARUS flux to the right of μBooNE and finally the interaction parameter uncertainties are displayed in the right-most 19 bins. These interaction uncertainties are identical for every experiment in the SBN program.

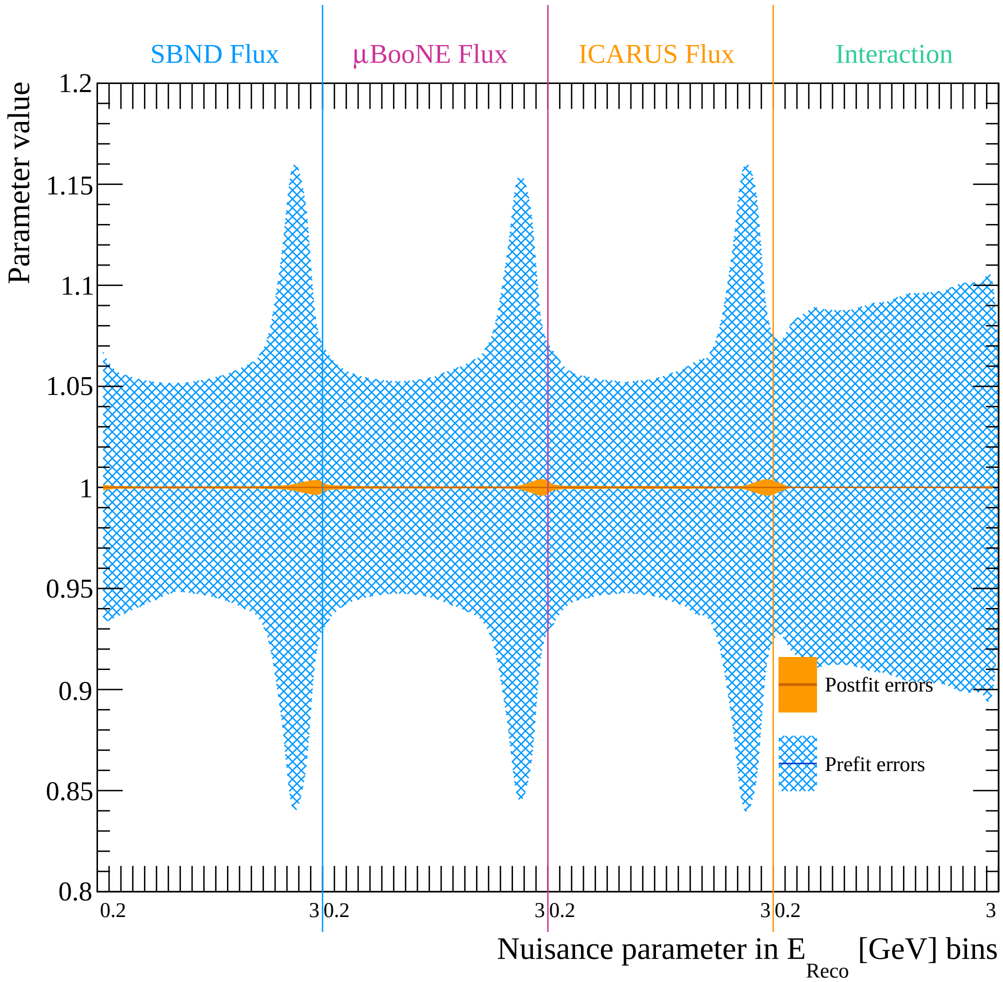

Figure 22: The prior & postfit uncertainties on the nuisance parameters defined in Table 5 overlaid for direct comparison. The prior uncertainties here were taken directly from the input covariance matrix generated by the VALOR fitting framework. The postfit uncertaintes are the result of a fit between the MC and a toy prediction generated using the same MC sample, consequently they have been highly constrained and are very small. The SBND flux parameter uncertainties are in the left 19 bins, μBooNE flux in the following 19 bins, ICARUS flux to the right of μBooNE and finally the interaction parameter uncertainties are displayed in the right-most 19 bins. These interaction uncertainties are identical for every experiment in the SBN program.

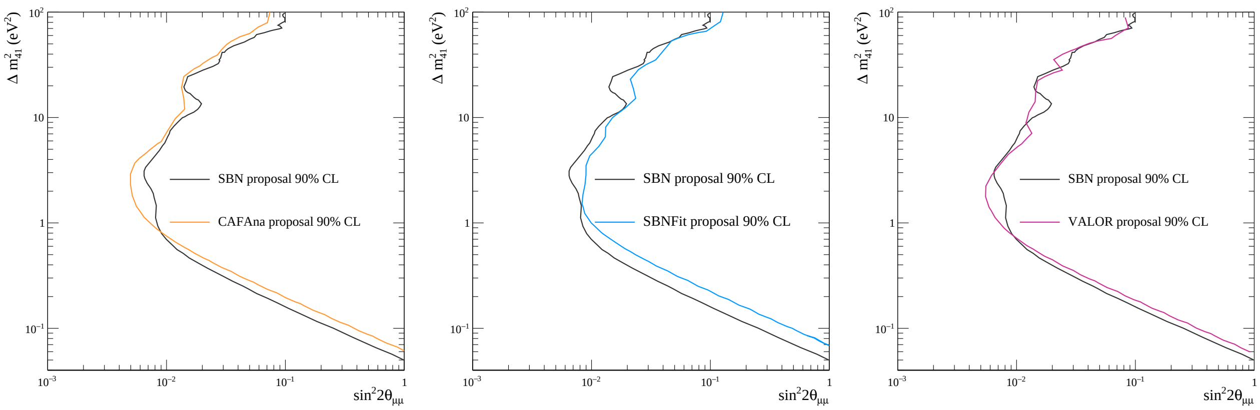

Figure 23: Muon Neutrino disappearance exclusion contours produced by each of the three fitting frameworks. From left to right: CAFAna, SBNFit, VALOR. Included in each plot is a contribution from the proposal-style sample with statistical+systematic uncertainties. Each are compared to the analogous contour produced for the SBN proposal in 2015 (black line). All are shown at the 90% C.L.

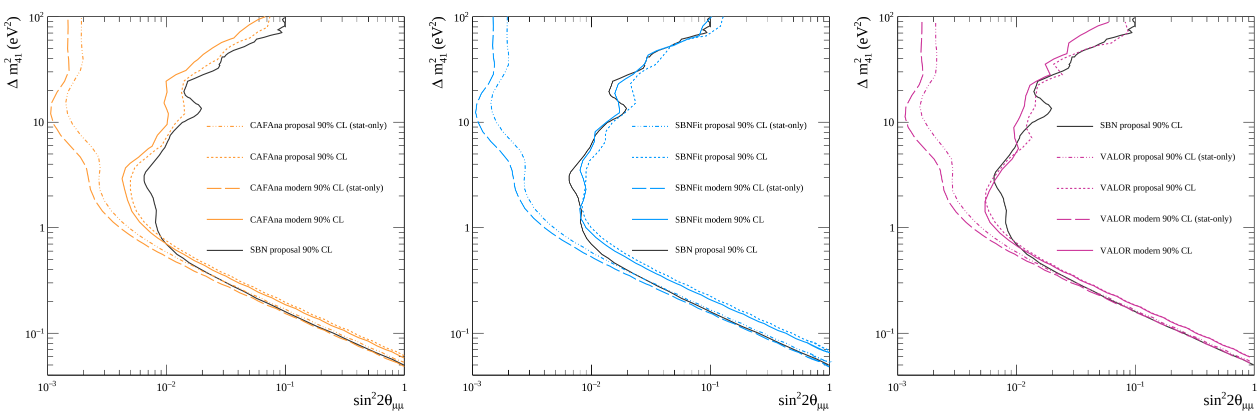

Figure 24: Muon Neutrino disappearance exclusion contours produced by each of the three fitting frameworks. From left to right: CAFAna, SBNFit, VALOR. Included in each plot is a contribution from both the modern and proposal-style samples along with the consideration of statistical-only and statistical+systematic uncertainties. Each are compared to the analogous contour produced for the SBN proposal in 2015 (black line). All are shown at the 90% C.L.

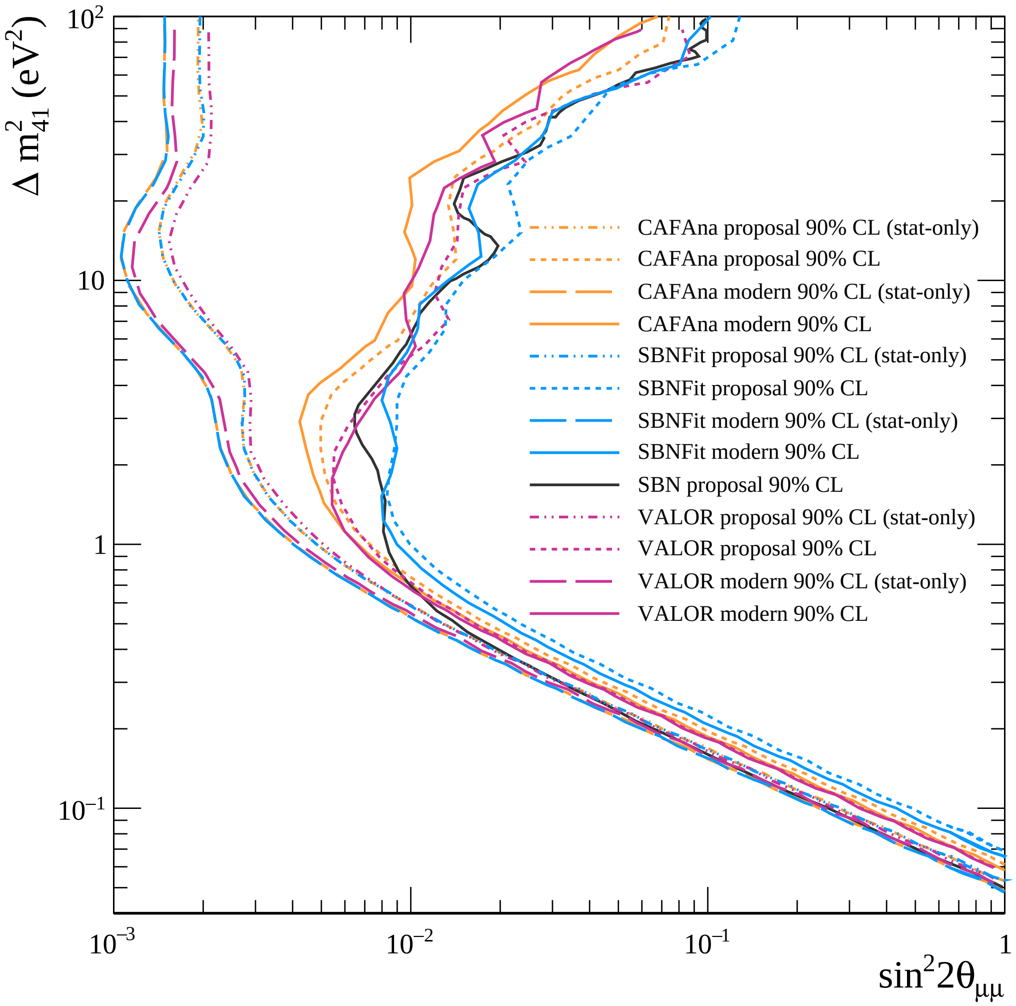

Figure 25: Muon Neutrino disappearance exclusion contours produced by each of the three fitters, this time presented in a single plot for direct comparison. Once again, included in each plot is a contribution from both the modern and proposal-style samples along with the consideration of statistical-only and statistical+systematic uncertainties. Each are compared to the analogous contour produced for the SBN proposal in 2015 (black line). All are shown at the 90% C.L.

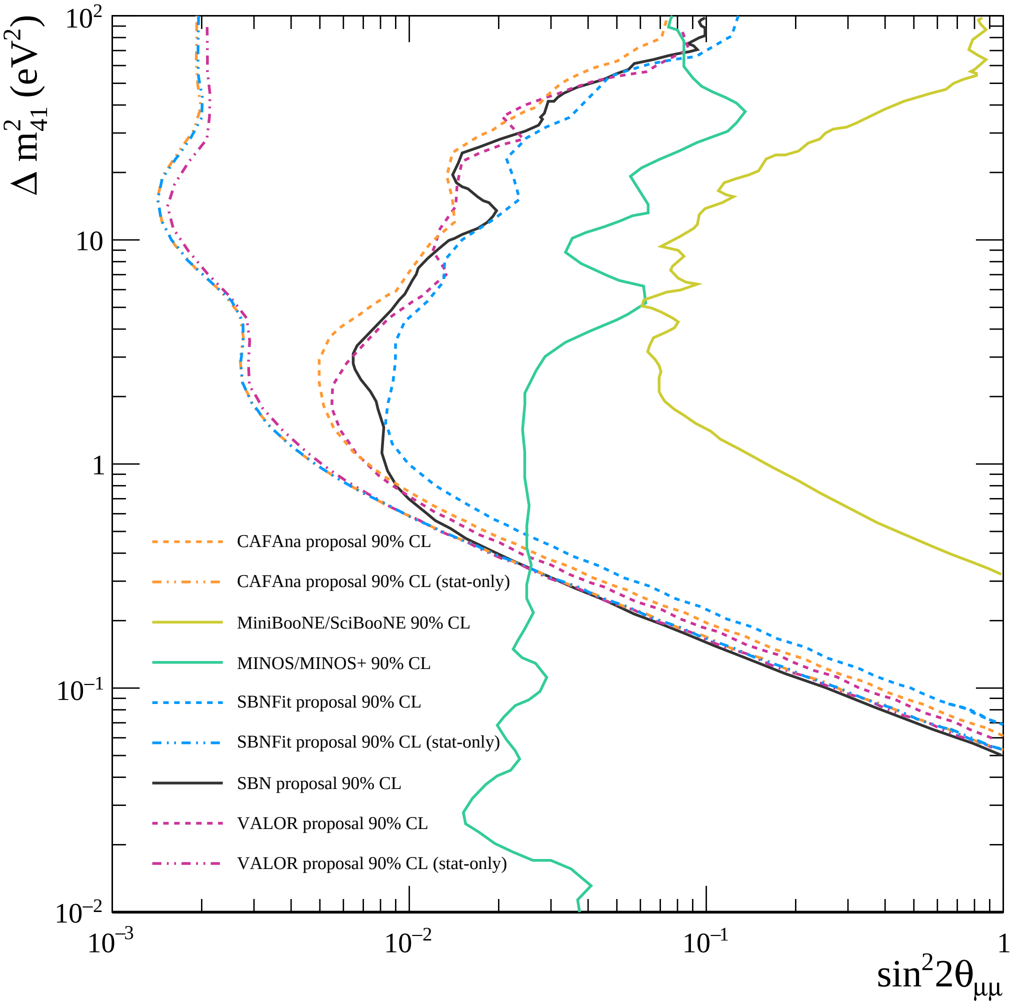

Figure 26: Muon Neutrino disappearance exclusion contours produced by each of the three fitters using the proposal-era samples. Once again statistical-only and statistical+systematic uncertainties are considered by the fitters. Each are compared to the analogous contour produced for the SBN proposal in 2015 (black line) along with the MINOS (teal) and MiniBooNE (yellow) results at the 90% C.L.

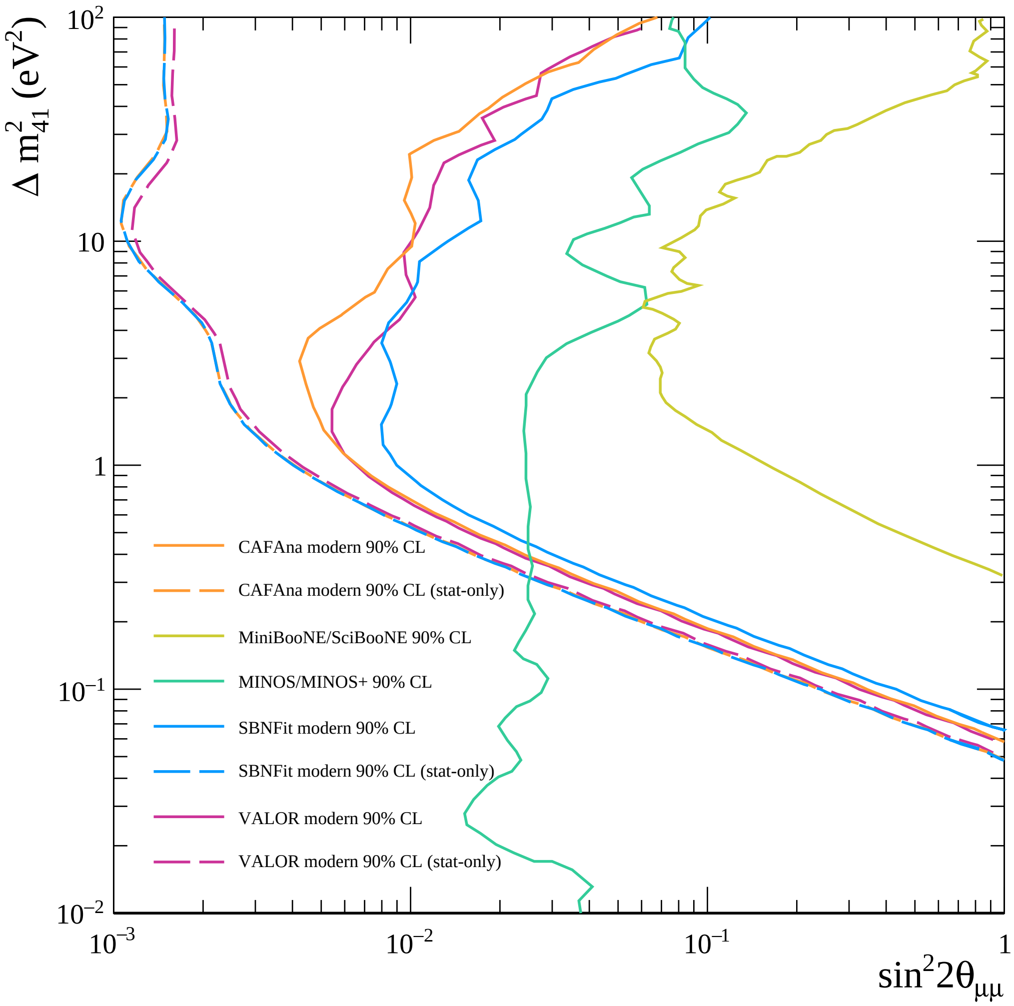

Figure 27: Muon Neutrino disappearance exclusion contours produced by each of the three fitters using the up-to-date, modern samples. Once again statistical-only and statistical+systematic uncertainties are considered by the fitters. These sensitivities are presented alongside the MINOS (teal) and MiniBooNE (yellow) results at the 90% C.L.

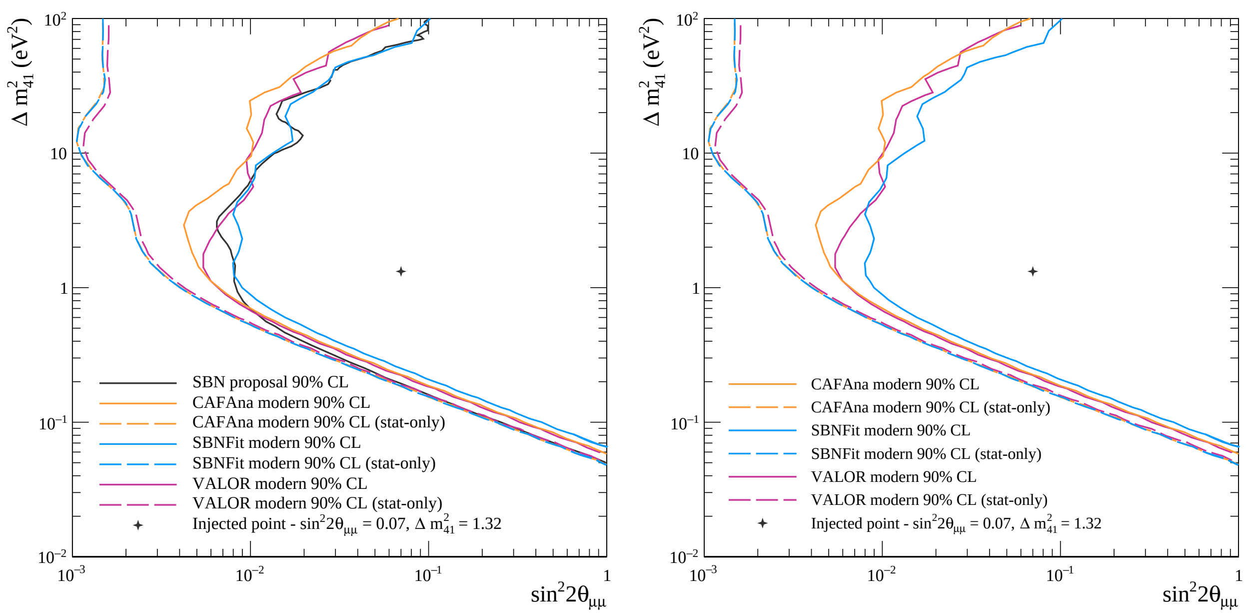

Figure 28: Muon Neutrino disappearance exclusion contours produced by each of the three fitters using the up-to-date, modern samples. Once again statistical-only and statistical+systematic uncertainties are considered by the fitters. These sensitivities are presented alongside the SBN proposal contour from 2015 (black line) on the left, without the proposal on the right. The injection point corresponding to that which was used to produce allowed regions in Figures 31, 33, 32 & 35 is included for context. Results at the 90% C.L.

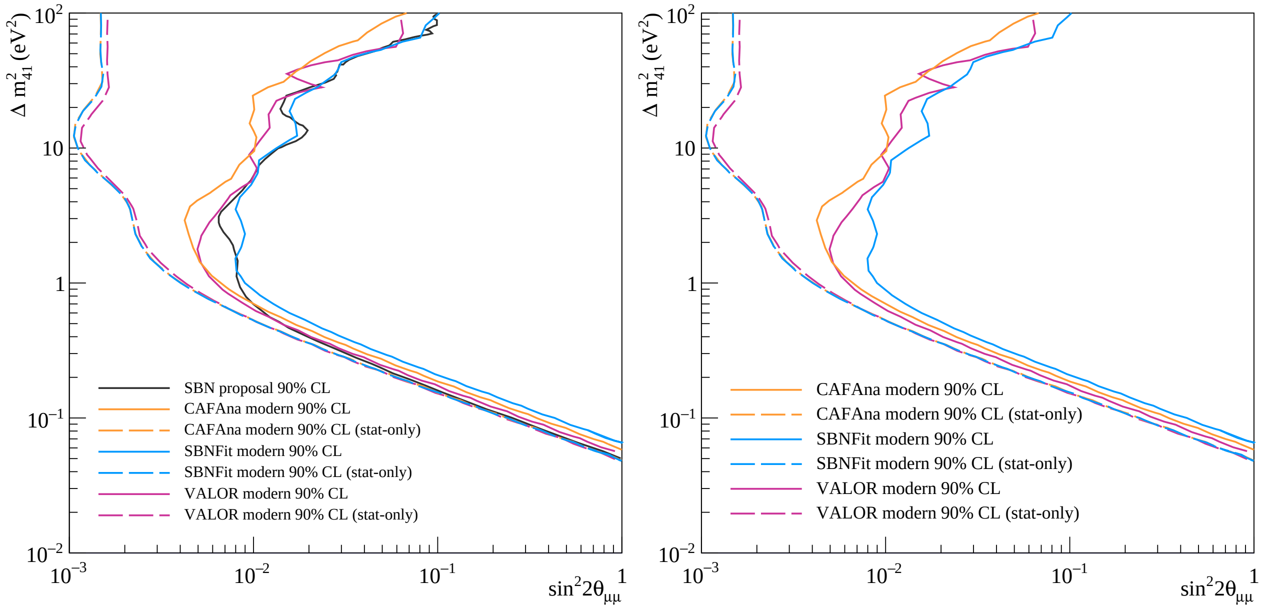

Figure 29: Muon Neutrino disappearance exclusion contours produced by each of the three fitters using the up-to-date, modern samples. Once again statistical-only and statistical+systematic uncertainties are considered by the fitters. These sensitivities are presented alongside the SBN proposal contour from 2015 (black line) on the left, without the proposal on the right. Results at the 90% C.L.

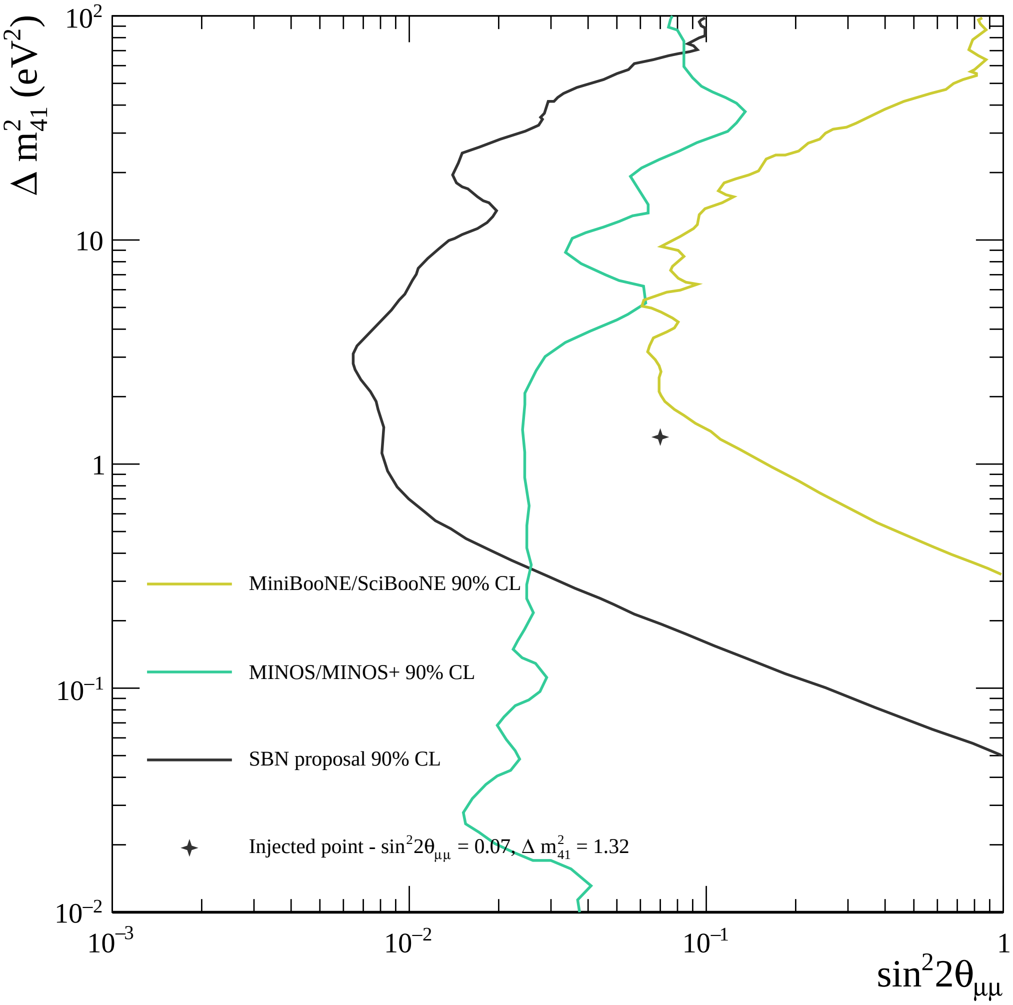

Figure 30: Muon Neutrino disappearance exclusion contours produced for the SBN proposal in 2015 along with the results from the MINOS/MINOS+ & MiniBooNE/SciBooNE experiments. The injected point used to produce the following allowed-region contours (Figures 31, 32, 33, 34 & 35) is also shown in context with these exclusion contours. Results at the 90% C.L.

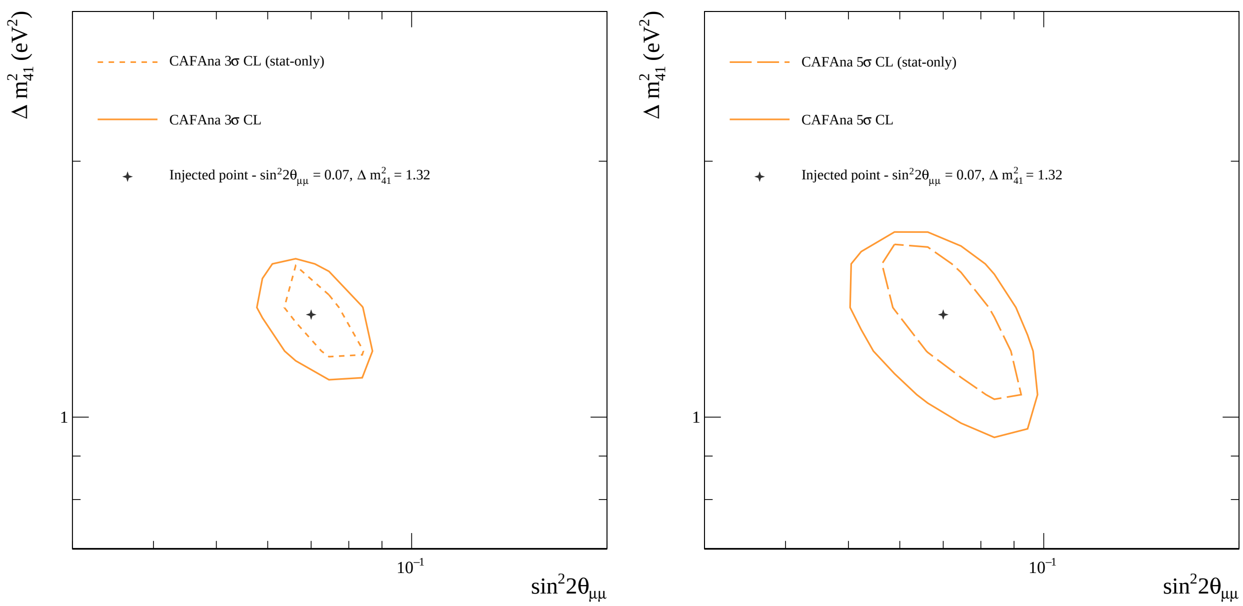

Figure 31: Muon Neutrino disappearance allowed regions produced by the CAFAna fitting framework. Included in each plot is a contribution from the modern-style samples along with the consideration of statistical-only and statistical+systematic uncertainties. The left hand plot shows the 3σ C.L. allowed region while the right shows the 5σ C.L.

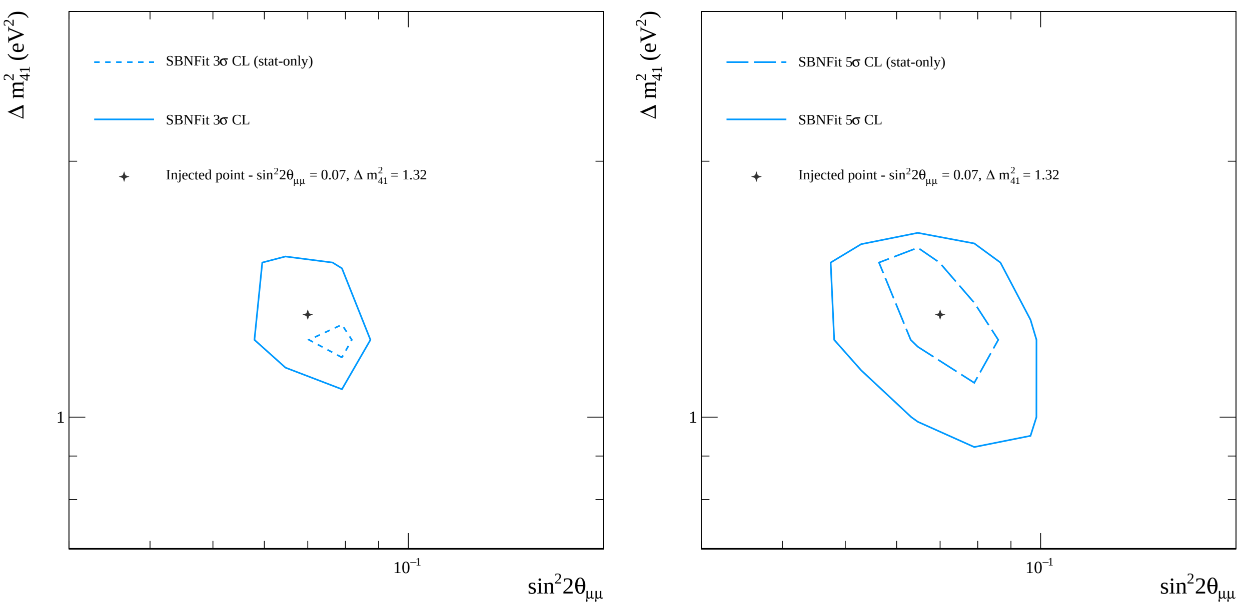

Figure 32: Muon Neutrino disappearance allowed regions produced by the SBNFit fitting framework. Included in each plot is a contribution from the modern-style samples along with the consideration of statistical-only and statistical+systematic uncertainties. The left hand plot shows the 3σ C.L. allowed region while the right shows the 5σ C.L.

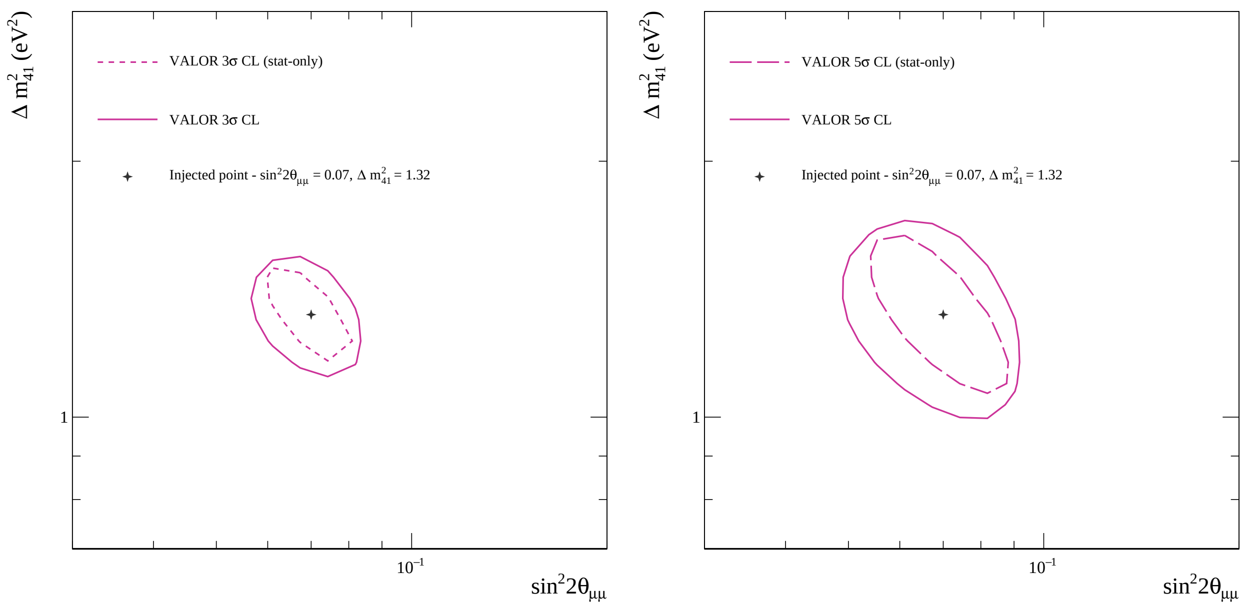

Figure 33: Muon Neutrino disappearance allowed regions produced by the VALOR fitting framework. Included in each plot is a contribution from the modern-style samples along with the consideration of statistical-only and statistical+systematic uncertainties. The left hand plot shows the 3σ C.L. allowed region while the right shows the 5σ C.L.

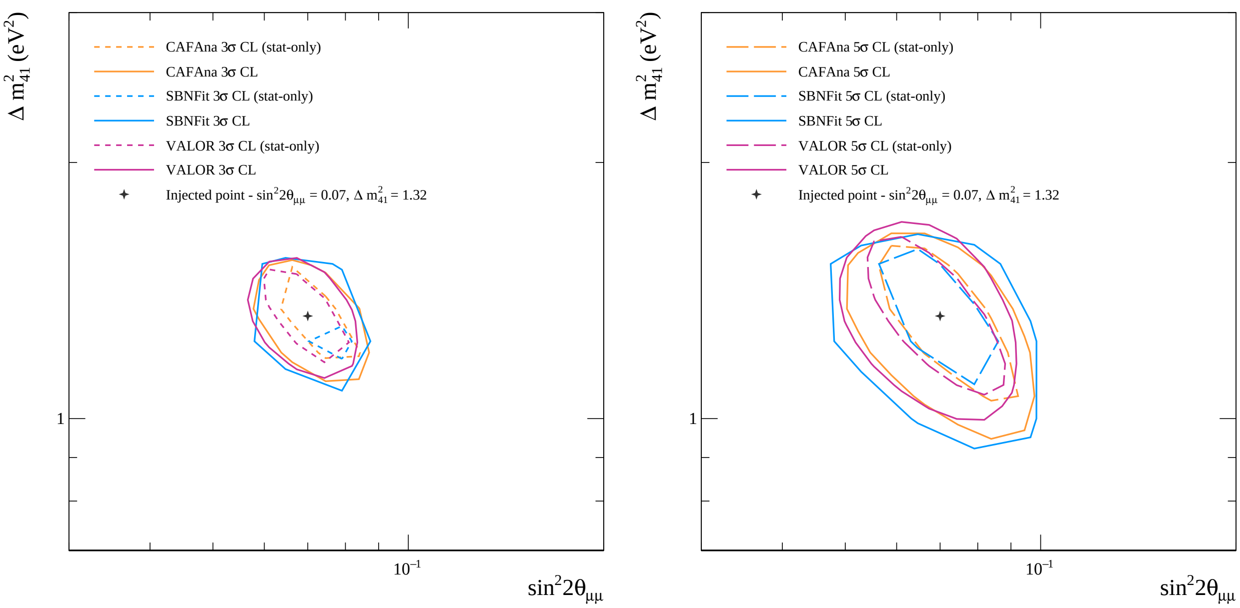

Figure 34: Muon Neutrino disappearance allowed regions produced by the CAFAna, SBN-Fit & VALOR fitting frameworks. Included in each plot is a contribution from the modern-style samples along with the consideration of statistical-only and statistical+systematic uncertainties. The left hand plot shows the 3σ C.L. allowed region while the right shows the 5σ C.L.

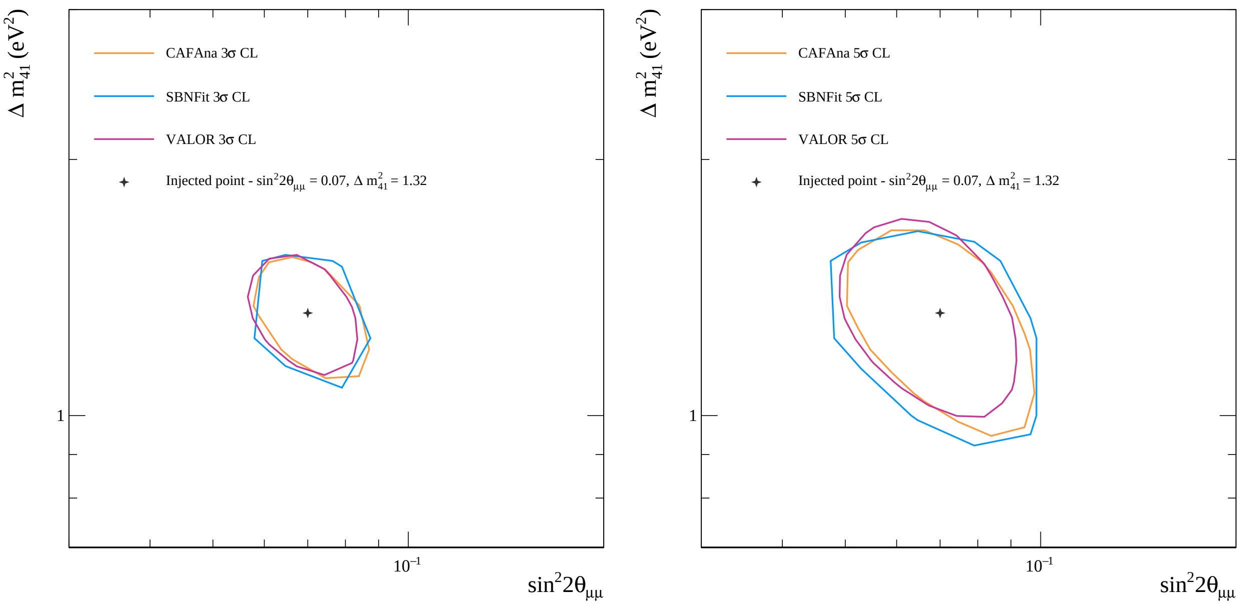

Figure 35: Muon Neutrino disappearance allowed regions produced by the CAFAna, SBNFit & VALOR fitting frameworks. Included in each plot is a contribution from the modern-style samples along with only a consideration of statistical+systematic uncertainties. The left hand plot shows the 3σ C.L. allowed region while the right shows the 5σ C.L.